LUND UNIVERSITY

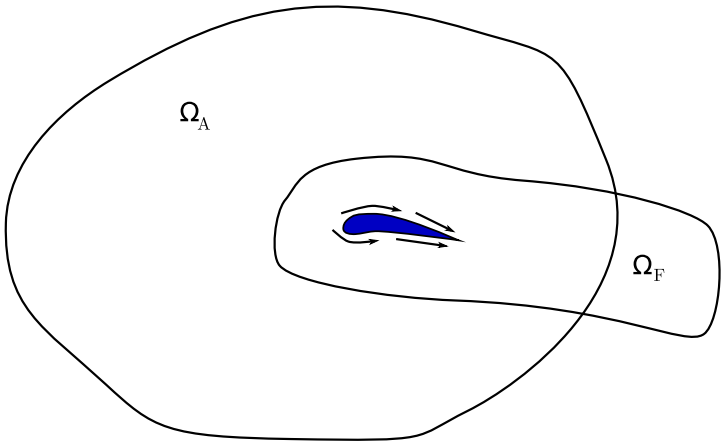

IMPLEMENTATION OF ACOUSTICAL ANALOGIES IN OpenFOAM AND CALFEM

JOHAN NILSSON

Engineering Acoustics

Master's Dissertation

Department of Construction Sciences
Engineering Acoustics

ISRN LUTVDG/TVBA--10/5040--SE (1-46)
ISSN 0281-8477

IMPLEMENTATION OF ACOUSTICAL ANALOGIES IN OpenFOAM AND CALFEM

Master's Dissertation by

JOHAN NILSSON

Supervisors:

Per-Anders Wernberg, PhD,
Div. of Engineering Acoustics, Lund

Robert-Zoltan Szasz, PhD,
Dept. of Energy Sciences, Lund

Examiner

Delphine Bard, PhD,
Div. of Engineering Acoustics, Lund

Printed by Wallin & Dalholm Digital AB, Lund, Sweden, December, 2010 *(Pl)*.

For information, address:
Division of Engineering Acoustics, LTH, Lund University, Box 118, SE-221 00 Lund, Sweden.
Homepage: http://www.akustik.lth.se

Acknowledgments

The present work was carried out at the Division of Engineering Acoustics at Lund University, Sweden in 2010 in cooperation with Creo Dynamics.

I would like to thank my supervisor Per-Anders Wernberg for the support and guidance during the thesis and for introducing me to field of aeroacoustics. Further I would like to thank my other supervisor Robert-Zoltan Szasz for his support and long discussions about CFD. I would also like to thank Peter Davidsson for his assistance.

I would also like to take the opportunity to thank my family and friends for their support troughout my education.

The CFD simulations were performed on resources provided by the Swedish National Infrastructure for Computing (SNIC) at Lunarc, Lund University.

Abstract

Aeroacoustics is the field that studies flow induced sound. The source of sound can for example be fans, duct flows, aircraft propellers and objects mounted on the outside of a vehicle. The most often used computational methods for aeroacoustics are based on acoustical analogies.

The software package CALFEM is a finite element toolbox developed for teaching at Lund University. It contains routines to solve acoustical problems. OpenFOAM is an open source CFD code. In this master thesis it is investigated how a method using the acoustical analogies can be implemented with OpenFOAM and CALFEM.

The method was implemented as follows. First, an incompressible flow simulation is carried out using OpenFOAM which provides the acoustic sources. Then the source terms are interpolated and converted for use in CALFEM. This was done by adding code to OpenFOAM, writing conversion programs and writing a CALFEM case.

Finally the implemented method was tested on an open cavity. Since it was difficult to find relevant experimental measurements, the method could not be properly validated yet.

Contents

Chapter 1

Introduction

1.1 Background

Aeroacoustics is the field that studies flow induced sound. Some aeroacoustic examples are the noise from a jet engine, wind turbines, music from wind instruments and telephone wires "singing" in the wind. Aeroacoustics has mainly been used to reduce the noise from jet airliners, but other uses are starting to become important as well. One example is car manufacturers that have been able to reduce engine and tire noise so that aerodynamic noise becomes dominant at high speeds. Even at lower speeds climate systems also generate a lot of aeroacoustic noise. [1, 2]

The subject of aeroacoustics was pioneered by James Lighthill in the 1950s [3]. By rewriting the governing equations of fluid dynamics he derived a wave equation including a source term caused by the instantaneous velocity fluctuations in the flow. This was later extended to take reflections by solid surfaces into account, including moving surfaces, by Ffowcs-Williams and Hawkings (FW-H) [4]. Initially these results were only used analytically, but with Computational Fluid Dynamics (CFD) it has become possible to extract the source terms from a CFD simulation. [1, 2]

The typical way to solve the acoustic wave equation is to integrate the sources using Green functions. These integral formulations use the free flow assumption. This may be suitable for a jet airliner, but for confined flows, such as a car climate control system this is not the case. To avoid the restriction of the free flow assumption a variational approach can be used with Lighthill's analogy. This was first presented by Oberai et al. in 2000 [5]. The equation is then discretized by using the Finite Element Method (FEM). This allows confined flows and more diverse acoustic properties to be assigned to the reflecting structures. In this approach the surface sources in FW-H:s formulation are taken care of by the FE solver instead of being explicit terms. [2, 6]

At the acoustics department at LTH there exists an extended version of CALFEM, a FEM software package that among other things performs acoustical analysis using either the FEM or the Boundary Element Method (BEM). It is of interest to be able to use this existing software for aeroacoustical phenomena as well and in general to learn about these hybrid methods in Computational Aeroacoustics (CAA).

1.2 Objectives

There are three main objectives of this thesis. The first is to study the theory to see how a hybrid CAA method can be used with CALFEM. The second is to implement such a method to extract the acoustical sources from a CFD software and make the conversions necessary to use these as sources in CALFEM. In other words the whole process from CFD simulation to acoustical results should be prepared. The final objective is to setup a case where the implemented method is tested.

1.3 Outline

The rest of the report follows the following structure.

- In chapter 2 the theory for the hybrid method is presented. This includes a derivation of Lighthill's source term and the FEM formulation of the acoustical problem. Other CAA methods are also presented and compared to the hybrid method that is the subject of this thesis.
- In chapter 3 this particular implementation of the method is described, including which software packages were used.
- In chapter 4 the test case, the open cavity, is described. Both the CFD and FEM models of the case and the general characteristics of the case are presented.
- In chapter 5 the results are presented.
- Finally the conclusions are discussed in chapter 6.

Chapter 2

Theory

2.1 Introduction to Hybrid CAA Methods

There are several challenges to overcome when attempting to compute aeroacoustical sound. Two of these are the large energy and length scale disparity. The energy in the flow is much greater than the energy in the acoustical waves. To quote Crighton in [7], "If all the acoustic energy radiated in the 45-second take-off of a large jet transport were recovered, that energy would be about enough to fry one egg!". Compare that to the energy in the flow which is used to lift the whole large jet aircraft to get a sense of the energy disparity.

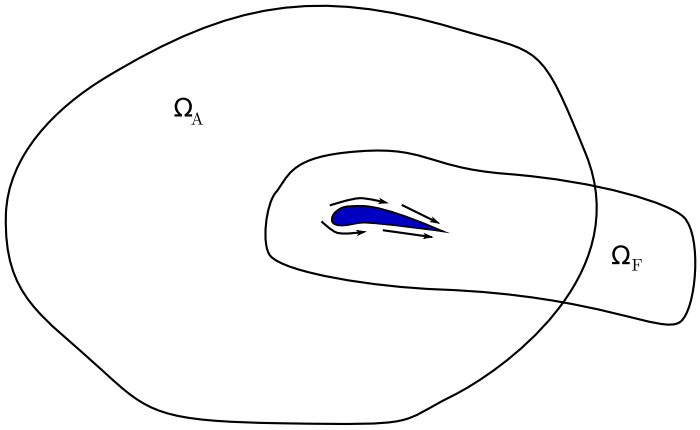

Figure 2.1: Domain partitioning of a typical CAA problem.

To deal with these difficulties hybrid methods are mostly used in Computational Aeroacoustics (CAA). These hybrid methods separate the computations for the flow and the acoustics. The flow simulation will be performed first. From the computed flow source terms will be computed for use in the acoustical computation. The advantage in separating the flow and the acoustic computation is that the two parts

can be setup differently. They can use different domains, meshes and time steps. Figure 2.1 shows how this is typically set up. The fluid domain Ω_F needs only to cover the area necessary to accurately capture the flow and the area that generates source terms. The fluid domain typically has a finer mesh than the acoustical domain. The acoustical mesh includes any objects that the user would like to include the effect of in the acoustical domain Ω_A. The fluid and the acoustical domain does not need to cover the same space. Depending on the method's formulation the acoustical domain may or may not need to extend all the way to the observer. All the methods described here, except Direct Simulation in section 2.4.1, are hybrid methods. [2]

2.2 Lighthill's Acoustic Analogy

Much in the field of aeroacoustics are derived from Lighthill's acoustic analogy which he originally presented in 1952 [3]. The analogy can be derived from the governing equations of fluid dynamics, the continuity equation and the momentum equation, here presented in conservative form using index notation. They are

$$\frac{\partial \rho}{\partial t} + \frac{\partial \rho u_i}{\partial x_i} = 0 \tag{2.1}$$

$$\frac{\partial \rho u_i}{\partial t} + \frac{\partial \rho u_i u_j}{\partial x_j} = -\frac{\partial p}{\partial x_i} + \frac{\partial \tau_{ij}}{\partial x_j} \tag{2.2}$$

where τ_{ij} are the viscous stresses, ρ, u_i and p are the fluid's density, velocity and pressure respectively. In the momentum equation the body forces are assumed to be zero. Now take the time derivative of (2.1) and then subtract the divergence of (2.2) to obtain the following scalar equation.

$$\frac{\partial^2 \rho}{\partial t^2} - \frac{\partial^2 \rho u_i u_j}{\partial x_i \partial x_j} = \frac{\partial^2 p}{\partial x_i^2} - \frac{\partial^2 \tau_{ij}}{\partial x_i \partial x_j} \tag{2.3}$$

Continue by introducing the density and pressure fluctuations as $\rho' = \rho - \rho_0$ and $p' = p - p_0$ where ρ_0 and p_0 are the atmospheric values of density and pressure respectively. Subtract $c_0^2 \partial^2 \rho / \partial x_i^2$ from both sides and rearrange to obtain Lighthill's inhomogeneous wave equation for acoustic density fluctuations

$$\frac{\partial^2 \rho'}{\partial t^2} - c_0^2 \frac{\partial^2 \rho'}{\partial x_i^2} = \frac{\partial^2 T_{ij}}{\partial x_i \partial x_j} \tag{2.4}$$

$$T_{ij} = \rho u_i u_j + \delta_{ij}(p' - c_0^2 \rho') - \tau_{ij}. \tag{2.5}$$

where T_{ij} is Lighthill's stress tensor, δ_{ij} is the Kronecker delta and c_0 is the undisturbed speed of sound. Here it was used that $\partial^2 \rho_0 / \partial t^2 = 0$.

Until now no assumptions have been made, other than those that are made to obtain the continuity and momentum equations. Thus this is an exact equation including all physics. If the right hand side is assumed to be known and independent of the left hand side, this equation can be viewed as an inhomogeneous wave equation in an isotropic medium at rest. This means that all the sound propagation is separated from the sound generation. In other words the acoustic field can not effect the flow field. In general the acoustic and the flow fields can not be separated. One example when the acoustic field effects the flow is the so called 'booming' noise that can appear when driving a car with the sunroof open. It also ignores the effect the mean flow has on the acoustic wave propagation. In most flows with low Mach number, the assumption that the flow does not depend on the acoustics is useful and most aerodynamic modelling is based on this. [1]

With the assumption that the wave propagation is isentropic the relation $p' = c_0^2 \rho'$ can be used to rewrite the inhomogeneous wave equation in terms of p' below.

$$\frac{1}{c_0^2}\frac{\partial^2 p'}{\partial t^2} - \frac{\partial^2 p'}{\partial x_i^2} = \frac{\partial^2 T_{ij}}{\partial x_i \partial x_j} \tag{2.6}$$

If the viscous effects in the wave propagation and the compressible portion also can be neglected the source term can be approximated by

$$\frac{\partial^2 T_{ij}}{\partial x_i \partial x_j} \approx \frac{\partial^2 \rho u_i u_j}{\partial x_i \partial x_j} \tag{2.7}$$

This means that the effects of viscosity and heat conduction are expected to cause only a slow damping due to the conversion of acoustic energy into heat [2]. This was assumed by Lighthill but it took some thirty years for this to be confirmed as reasonable [8].

The simplification also remove the compressible portion of the stress tensor which Slimon et al shows in [9]. In this article the error is shown to be proportional to Ma^2 which means that the acoustic source term would begin to lose accuracy around the same time as incompressible solvers lose accuracy if the formulation in (2.7) is used. They also show how a Janzen-Rayleigh expansion (similar to a Taylor expansion) can be used to compensate for this when going to higher Mach numbers. To use an extended formulation a compressible solver has to be used. In compressible flow the assumption that the acoustic field is separated from the flow field also becomes weaker, thus making the approach of acoustic analogies more suited for sufficient low Mach numbers to be used with incompressible CFD solvers. In this thesis focus will be on low Mach numbers, thus making (2.7) a good approximation.

2.3 FEM Formulation of Lighthill's Acoustic Analogy

The acoustic solver uses a FEM formulation of Lighthill's inhomogeneous wave equation (2.6). Its derivation begins by multiplying a test function v and integrating over the whole acoustic domain Ω.

$$\int_\Omega v\left(\frac{1}{c_0^2}\frac{\partial^2 p'}{\partial t^2} - \frac{\partial^2 p'}{\partial x_i^2}\right)dV = \int_\Omega v\frac{\partial^2 T_{ij}}{\partial x_i \partial x_j}dV \tag{2.8}$$

After applying Green's theorem to the second spatial derivative of p' this gives the weak form of (2.6).

$$\frac{1}{c_0^2}\int_\Omega v\frac{\partial^2 p'}{\partial t^2}dV + \int_\Omega \frac{\partial v}{\partial x_i}\frac{\partial p'}{\partial x_i}dV = \int_{\partial\Omega} v\frac{\partial p'}{\partial n_i}dS + \int_\Omega v\frac{\partial^2 T_{ij}}{\partial x_i \partial x_j}dV \tag{2.9}$$

In the following FE-formulation the notation follows the one used by Ottosen and Petersson [10] and it follows the theory presented by Wernberg in [11].

First the finite element approximation using base functions is introduced.

$$p' = \mathbf{N}\mathbf{p},\ v = \mathbf{N}\mathbf{c} \tag{2.10}$$

where the $\mathbf{p}$ contains the nodal pressures, $\mathbf{c}$ the arbitrary nodal weights and $\mathbf{N}$ contains the finite element shape functions. Note that $\mathbf{p}$ and $\mathbf{c}$ are column matrices and $\mathbf{N}$ is a row matrix, all with a length equal to the amounts of nodes in the computational domain. Inserting this into (2.9) gives

$$\frac{1}{c_0^2}\int_\Omega \mathbf{N}^T\mathbf{N}dV\ddot{\mathbf{p}} + \int_\Omega (\nabla\mathbf{N})^T\nabla\mathbf{N}dV\mathbf{p} = \int_{\partial\Omega}\mathbf{N}^T\frac{\partial p'}{\partial n_i}dS + \int_\Omega \mathbf{N}^T\frac{\partial^2 T_{ij}}{\partial x_i\partial x_j}dV \tag{2.11}$$

This can also be expressed as

$$\mathbf{M}\ddot{\mathbf{p}} + \mathbf{K}\mathbf{p} = \mathbf{f}_s + \mathbf{f}_q \tag{2.12}$$

where

$$\mathbf{M} = \frac{1}{c_0^2}\int_\Omega \mathbf{N}^T\mathbf{N}dV,\ \mathbf{K} = \int_\Omega (\nabla\mathbf{N})^T\nabla\mathbf{N}dV, \tag{2.13}$$

$$\mathbf{f}_s = \int_{\partial\Omega}\mathbf{N}^T\frac{\partial p'}{\partial n_i}dS,\ \mathbf{f}_q = \int_\Omega \mathbf{N}^T\frac{\partial^2 T_{ij}}{\partial x_i\partial x_j}dV$$

In this thesis the FEM problem is solved in the frequency domain. To do this harmonic motion is assumed and the complex quantities are introduced

$$\mathbf{f} = \hat{\mathbf{f}}e^{i\omega t},\quad \mathbf{p} = \hat{\mathbf{p}}e^{i\omega t} \tag{2.14}$$

where $\hat{\mathbf{f}}$ and $\hat{\mathbf{p}}$ are the complex force and pressure amplitudes, i is the imaginary unit and ω is the angular frequency. If this is inserted into (2.12) and the $e^{i\omega t}$ are omitted for simplicity, the FEM formulation of the equations of motion becomes

$$(-\omega^2\mathbf{M} + \mathbf{K})\hat{\mathbf{p}} = \hat{\mathbf{f}}_s + \hat{\mathbf{f}}_q \tag{2.15}$$

In this thesis an absorbing boundary condition will be needed. The impedance Z is the relation between the fluid pressure and fluid velocity v

$$Z = \frac{p}{v_n} = \frac{p}{i\omega u_n} \tag{2.16}$$

where u_n is the fluid displacement in normal direction to the boundary. The relation between displacement and pressure can be written

$$\frac{\partial p'}{\partial n} = -\frac{i\rho_0\omega}{Z}p' \tag{2.17}$$

Apply this to the boundary term in (2.15) to get

$$\mathbf{f}_Z = -i\omega\int_{\partial\Omega_Z}\mathbf{N}^T\frac{1}{Z}p'dS = -i\omega\int_{\partial\Omega_Z}\mathbf{N}^T\frac{1}{Z}\mathbf{N}dS\hat{\mathbf{p}} \tag{2.18}$$

In the last step the finite element approximation was applied to p'. Due to this it makes now sense to define the impedance matrix $\mathbf{C}$ as

$$\mathbf{C} = \int_{\partial\Omega_Z}\mathbf{N}^T\frac{1}{Z}\mathbf{N}dS \tag{2.19}$$

This will give the modified system of equations

$$(-\omega^2\mathbf{M} - i\omega\mathbf{C} + \mathbf{K})\hat{\mathbf{p}} = \hat{\mathbf{f}}_s + \hat{\mathbf{f}}_q \tag{2.20}$$

2.4 Other CAA methods

2.4.1 Direct Simulation

The conceptually easiest way to compute sound would be to solve the set of governing equations (which in addition to (2.1) and (2.2) also includes the heat equation and some constitutive relations [1]) directly without any modelling. This is called Direct Simulation (DS). In CFD the equivalent is known as Direct Numerical Simulation (DNS). While it can produce the most accurate results the computational costs are very high and it increases with Reynolds number approximately as Re^3. This makes the situations where DNS can be used very limited [12]. In addition to resolving the Kolmogorov length scale as necessary by DNS all acoustic waves must also be resolved in DS. This is even expensiver as the computational costs scale

approximately as $Ma_t^{-4}Re^3$, where Ma_t is the turbulent Mach number defined as $Ma_t = U_{rms}/a$ where a is the speed of sound and U_{rms} is the root mean square value of the instantaneous velocity. In addition it is important that the numerical scheme has low dissipation so that it doesn't damp out the acoustical waves. Because of these facts, the possibility to separate the acoustic field from the flow field becomes attractive, for example using the method of acoustic analogies studied in this thesis. [1]

2.4.2 Integral Formulations of Acoustic Analogies

Lighthill's inhomogeneous wave equation (2.6) can, if the right hand side is assumed to be known, be solved analytically using a free space Green's function integrating over all of space. This assumes that the sound can radiate freely from its distribution of sources including no solid boundaries that could affect the wave propagation. For jet noises this may be useful, but in many cases solid surfaces needs to be considered. [2, 8]

The integral formulation was extended to account for solid and moving surfaces by Ffowcs Williams and Hawkings (FW-H). FW-H did this by applying generalized functions to the derivation of Lighthill's analogy. This gives a thickness loading term acting as a monopole source, a surface loading term acting as a dipole and the same term as in the integral formulation of Lighthill's analogy acting as a quadrupole term. The monopole and dipole terms are only integrated on the surfaces that are taken into account. [1, 2]

There are also other formulation based on FW-H's, often trying to overcome one or more of the issues described here or in the following subsection. [1]

2.4.3 Comparison Between Integral and Variational Formulations of Acoustic Analogies

In comparison to a variational formulation, such as the one described in the previous section, formulations such as FW-H's handles reflections explicitly in separate terms. These methods can be implemented in a Boundary Element Method code to deal with confined problems. In the surface terms pressure fluctuations must be provided by the CFD simulation, but in most applications the information isn't accurate enough on all walls to obtain a good result [13]. Oberai et al. also found that the requirements on the resolution on the velocity field, the only field used in Lighthill's equation, to be far lower [5].

A variational formulation instead handles the interactions with solid surfaces implicitly by the acoustic solver. This makes it possible to include more complex

interactions between the fluid and the structure and can perform better with confined flows. There is however no separation between the different contributions like there is in the integral methods. The integral formulations are suited for computing the sound level at a few points far away from a compact object since the entire domain does not need to be discretized. The variational formulation on the other hand gives the solution to the whole computational domain at once but must discretize the entire domain up until the point where the sound level is requested. Also ending the domain can require special more complicated techniques for free flow problems in a variational formulation. [2, 6, 13]

2.4.4 Systems of Equations

The acoustic analogies discussed above have solved the fluid dynamic and taken the result as a source in a scalar acoustic equation. This has, as mentioned above, the effect that some physics are left out. In order to retain more physics in the acoustic part of the simulation, there are several methods that solves a system of equations instead of just one scalar equation in the acoustic computation. One obvious drawback is that it is more complex and expensive to solve several equations than just one. [1]

The equations used can be derived from the linearized Euler equations (LEE) which are solved for perturbation quantities. This is done by reasoning that the propagation of sound waves are nearly inviscid and that the amplitudes of the perturbations are very small which means the equations can be linearized. This approach takes into effect mean flow effects such as refraction. However when using LEE one has to somehow deal with growing instability waves. [14, 15]

One approach called Expansion about Incompressible Flow (EIF), suggested by Hardin and Pope, assumes that the flow field will be computed from a incompressible CFD. This assumption is then used as basis for the acoustic equations. This approach is analyzed by Slimon et al. in [9]. Other examples of systems of equations are Acoustic Perturbation Equations (APE) proposed by Ewert and Schröder [16] and Perturbed Compressible Equations (PCE) and its linearized version LPCE proposed by Seo and Moon [17].

Chapter 3

Implementation

3.1 Overview

In this thesis the FE formulation of Lighthill's analogy is used in combination with a CFD simulation. An overview of the the method is sketched in Figure 3.1. First a CFD simulation on the problem geometry is performed. From the CFD simulation the acoustical source term is computed by using equation (2.7). After interpolating the sources from the CFD mesh to the acoustical FEM mesh these sources will be used as input to the acoustical FEM solver (CALFEM).

The mesh in the CFD and FEM computations need not be the same. The two different meshes need not cover the same regions either. The CFD domain does only need to cover the area where sound generation occurs (besides everything that is relevant for the flow) and the acoustic domain need only cover what is of interest for the acoustical simulation.

To accommodate two different meshes some form of interpolation needs to be used to transfer the sources to the acoustical mesh. In this thesis acoustical problem will be solved in the frequency domain, which adds one more step in the conversion. However, the general principles of the method does not require this. The next step is using the FEM solver to solve for the acoustic pressure fluctuations. Finally these will be used to determine the sound pressure levels.

The rest of this section describes how the method has been implemented. In section 3.2 the CFD software used, OpenFOAM, is described and in section 3.3 the FEM software used for the acoustics CALFEM is presented. The implementation of the acoustical source terms in OpenFOAM is described in section 3.4. For the interpolation between the fluid and acoustical meshes the OpenFOAM utility `mapFields` was used. To be able to use `mapFields` both meshes needs to be available in OpenFOAM format. This was solved by generating both meshes in OpenFOAM and writing a program to convert the acoustical mesh from OpenFOAM to CALFEM. This mesh

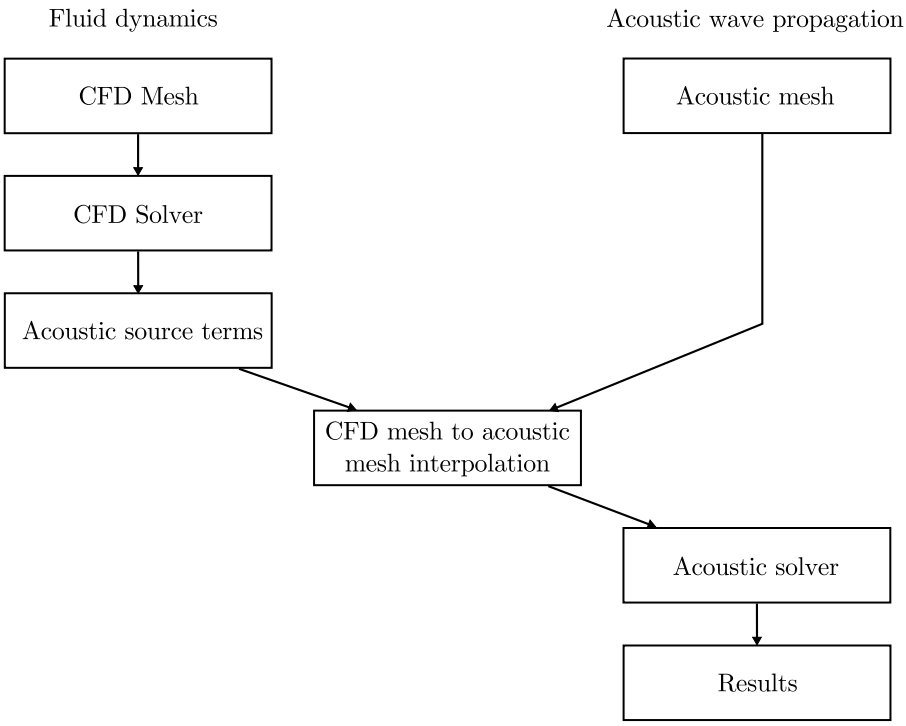

Figure 3.1: Overview of the implemented method.

converter is described in section 3.5. Some words on the interpolation are given in section 3.6. Since the acoustical solver works in the frequency domain the acoustical source terms needs to be transformed from the time domain. It also needs to be converted to CALFEM format since the mesh converter only converts the mesh and no data. The data transformation and conversion is described in section 3.7.

3.2 OpenFOAM

For the CFD simulations the software package OpenFOAM, version 1.6.x, was used. OpenFOAM (Open Field Operation And Manipulation) is a free, open source package produced by a commercial company, OpenCFD Ltd. The code is written in advanced C++ and makes heavy use of the object oriented programming model, for example relying heavily on templates. It includes some rather simple meshing tools (but can import many formats), many CFD and some other solvers, a third party post-processor and other utilities. [18]

OpenFOAM was chosen for several reasons. First, since it is free of charge and is licensed under the GNU General Public License ver. 3 (see [19] for more about the GPLv3) any otherwise potential cost and licensing issues does not exists. Secondly, since it is open source it can "easily" be modified to the user's needs, for example to extract source terms. With easily means that since the user is free to do

modifications (which may not be the case in proprietary software) and that there are prepared libraries that can greatly simplify the process. It does often however require some time to understand how the code is structured and some knowledge about advanced C++ certainly helps.

3.3 CALFEM

CALFEM ("Computer Aided Learning of the Finite Element Method") is a FEM software package developed at the Division of Structural Mechanics, Lunds University since the late 70's for teaching the finite element method. It can be used for different type of structural mechanics and field problems [20]. CALFEM is written as a collection of MATLAB .m files, however recently it has also been ported to Python as Ottoson's master thesis [22]. CALFEM is distributed under the GPL (see [19]) and can be found at [21]. In this thesis however, a modified and extended version of CALFEM was used. This version extends CALFEM's capabilities, such as adding more possibilities to connect to other programs like Nastran, adding more boundary conditions and optimizing some routines. From the extended and modified parts routines for the impedance boundary condition described in section 2.3 and an optimized assembly procedure was used in this thesis.

3.4 Implementation of Source Term in OpenFOAM

At the time of making this thesis OpenFOAM did not include any code that computed the acoustic source term. But thanks to OpenFOAM's object oriented structure, most work was already taken care of. There are a set of classes that handles fields of any kind (scalar, vector or tensor). The source term field was simply declared as a scalar field with a few properties such as dimension and I/O control. There are also pre-defined operations on these general fields such as divergence which has been used in the source term calculation. The framework also allows the discretization (for example for the divergence operation on a given field) to be chosen at run time. It does not only saves the programmer a lot of work, but the code also becomes compact and easy to understand. [18]

The source code shown in listing 1 was added near the end of each time step of the solver used. The first line and the if statement controls whether the acoustic source terms should be computed this time step. Since the data amount can be very large, the possibility to control the frequency for source term output independently of other field's output gives more control of the disk space requirements. The first and last line inside the if statement are output for the log file, the second line computes the source term according to (2.7) and the third line writes it to disk. In addition to

this some lines were added to `createFields.H` file that is referenced in the solver's source code. These lines read the variables `rho` and `sourceWriteTime` from a so called dictionary (input file in OpenFOAM) and also constructs the source term field `acoSor`. To control disk space usage some additional modifications to the output control was also made.

```
const double kvot = runTime.timeOutputValue() / sourceWriteTime;
if(fabs(kvot - floor(kvot+0.5)) < 1e-8)
{
    Info << "Begin computing acoustic source terms" << endl;
    acoSor = rho * fvc::div(fvc::div(U*U));
    acoSor.write();
    Info << "End computing acoustic source term" << endl;
}
```

Code listing 1: The code that computes the acoustic source terms.

3.5 Mesh Converter

As described in the section 2.1 the meshes in the acoustical and fluid domain do not need to be the same. The two simluation parts can also be solved in two different programs. In this thesis these are OpenFOAM and CALFEM as already mentioned. These two programs uses different formats for handling the mesh. To facilitate the data conversion and interpolation a mesh converter was written, converting OpenFOAM's mesh format to a mesh in CALFEM format. Using this converter both meshes could be generated in OpenFOAM and the interpolation tool `mapFields`, which is a part of OpenFOAM, could be used when interpolating the data. The data interpolation process itself is presented in section 3.6.

The two different programs handles the meshes differently. In CALFEM one cell consists of a set of nodes in a specific order. In OpenFOAM the structure is a bit more complex. One side of a cell, called a face, consists of a set of nodes grouped similarly as a CALFEM cell. Each face then belongs to a cell and, unless it is a boundary face, has a neighbour. Fortunately both mesh formats are documented which made the writing of mesh converter feasable.

The mesh converter only supports hexahedral 3D elements with 8 nodes. Extending the converter to support more element types should not be particularly difficult since the general principles of the two formats have already been dealt with once. A separate program that extracts the surface elements on a given boundary from OpenFOAM and converts them to CALFEM format was also written. This was used for setting the impedance boundary condition in CALFEM. A converter from CALFEM format to OpenFOAM format was also written, but not used in the computational method presented in this thesis.

3.6 Data Interpolation

In order to be able to run the acoustic solver, the data has to be transferred to the acoustic solver and the acoustic mesh. Since the meshes are different the nodes does not need to be located in the same positions and the number of nodes can also be different. Also the two meshes does not need to cover the same volume. All of these differences exist in the case tested and needs to be handled in some way. Fortunately this kind of mesh transfer is not a too unusual operation in CFD. To this end, OpenFOAM comes with the utility `mapFields` which is made specifically for the purpose of interpolating fields between different meshes. `mapFields` meets all the requirements listed above. The tool was slightly modified so it would do all timesteps in one single run.

At some point the acoustical sources needs to be computed. One question is if it should be done prior to interpolating the data to the acoustical mesh or after the data has been interpolated. This was investigated by Escobar [2]. He used a finer mesh in the CFD simulation than the acoustical simulation and he concluded that best results were obtained if the acoustical sources are computed on the CFD mesh before the mesh interpolation takes place. This is also how it is done in this thesis. In general the CFD mesh is expected to be the finer of the two meshes.

In the FEM formulation presented in section 2.3, the sources appear as a load vector. These are applied in CALFEM as nodal loads analogous to applying nodal forces in a solid mechanics problem. OpenFOAM uses a finite volume discretization where the value of the sources are stored at each cell center. These cell center values can then be interpolated with neighbouring cells to estimate the value at an arbitrary point. If these sources are to be concentrated to the nodes only, they must be integrated somehow. This was done by the simple method of assigning one eighth of the cell center value to all nodes of the cell, thus making the integration conservative. In OpenFOAM terminology this would be a `volumeField` to `pointField` interpolation. A short program was written to perform this.

3.7 Time to Frequency Domain Transformation

Since the acoustical solver works in frequency domain and the CFD solver works in the time domain the data transferred between the solvers (the acoustical source terms) needs to be transformed. This is done by computing the Discrete Fourier Transform (DFT) of the source terms in each node. Computing the DFT directly from its definition is computationally very expensive. Instead an approximate algorithm is usually used. These algorithms are called the Fast Fourier Transform or FFT and there are many different FFT:s. In this thesis the FFTW algorithm version 3.2.2 was chosen [23]. FFTW stands for “Fastest Fourier Transform in the

West". It comes as a C library and has a GPL license or a commercial license. For example FFTW is used by Matlab [24].

The FFTW library is used in a pretty straight forward way. The time signal of each node is given to FFTW which transforms it to the frequency domain. Since the phase information can be crucial for interference effects between acoustical waves both amplitude and phase information are transferred to the acoustical solver. One program was written to handle the time to frequency domain transformation. It also converts the data (not to confuse with the mesh) from OpenFOAM to CALFEM format. This program is the final step performed before running the acoustical solver. This means that this program is run after the sources has been interpolated to the acoustical mesh.

Chapter 4

Description of Case

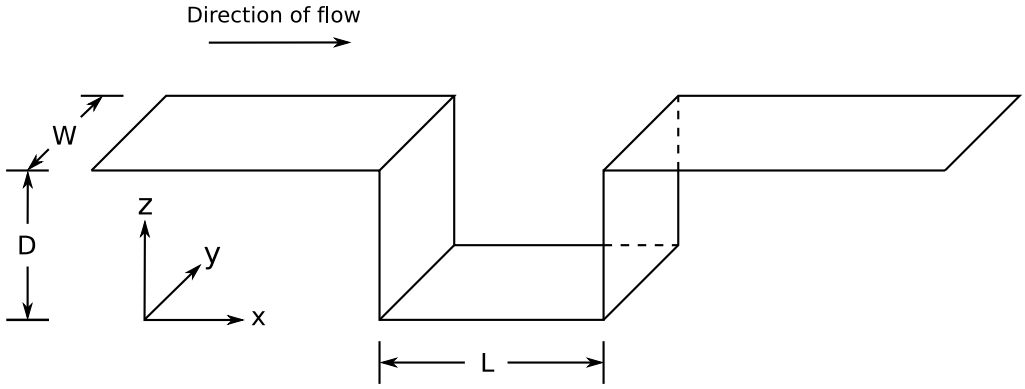

Figure 4.1: Cavity geometry.

4.1 Overview

To validate the method that is the subject of this thesis a open cavity was chosen as a test case. The geometry is given in Figure 4.1. The open cavity was chosen for a number of reasons. It has been studied quite a lot in the literature. The simple geometry makes the block meshing tool in OpenFOAM sufficient (no external meshing tool was needed) and despite its simple geometry it creates interesting and complex phenomena. This kind of cavity is known to be the source of strong acoustic fields causing acoustic fatigue in aeroplanes and in general causing a lot noise [25], thus giving some real world relevance.

4.2 Open Cavity Flow

As mentioned above there have been many investigations about the open cavity. Depending on the problem parameters the flow can be divided into three different flow regimes, no oscillations, shear regime and wake regime. These regimes are often called modes but in this thesis the terminology (suggested by Larsson [1]) will be regime. This is done to avoid confusion with the Rossiter modes in the shear regime. The most important parameters for determining the flow character appears to be the length L to depth D ratio (L/D) and the boundary layer thickness δ to length ratio (δ/L) [1]. If the boundary layer is thick enough there will be no oscillations. When the δ/L ratio decreases oscillations will occur in the cavity which is called the shear regime. If the boundary layer is further thinned the flow will eventually switch to wake regime. [1, 26]

4.2.1 Shear Regime

The shear regime is characterized by self-sustained oscillations at one or a few distinct frequencies. These frequencies lie within certain bands which fairly well follow a semi-empirical formula developed by Rossiter [27]:

$$St_L = \frac{n - \alpha}{Ma + 1/\kappa}, \quad n = 1, 2, 3... \tag{4.1}$$

where St_L is the Strouhal number of the n-th mode frequency, Ma is the Mach number. The Strouhal number is the non-dimensionalized frequency and is defined as

$$St_L = \frac{fL}{U} \tag{4.2}$$

where f is the frequency, L is the cavity length and U is the free stream velocity. There are two empirical constants in Rossiter's formula, α is a phase delay and κ corresponds to the average convection speed of disturbances in the shear layer. These are normally set to $\alpha = 0.25$ and $1/\kappa = 1.75$, which are the original values used by Rossiter.

The oscillation phenomena is usually described as small disturbances in the shear layer at the leading edge of the cavity. These vortices or disturbances travel across the cavity and eventually reach the downstream cavity wall where it generates an acoustic wave. This wave then travels upstream to the leading edge where it triggers a new disturbance. At certain frequencies this periodic phenomena gives resonance. This theory is what Rossiter used when developing his formula (4.1). Also note the presence of the Mach number in (4.1). For incompressible flow the acoustic wave reach the leading edge instantly but for compressible flow the delay depends on the Mach number of the flow. [1, 28]

Rossiter's formula usually predicts the mode frequencies in experiments, but with significant scatter. The scatter is probably due to different experimental conditions. See for example [29] and [30]. Also the formula doesn't try to predict which mode will be excited. [28]

4.2.2 Wake Regime

The nature of the wake regime is far less studied than the shear regime. As the (δ/L) ratio decreases the shear regime will change into wake regime. In this mode the drag of the cavity increases dramatically. This was discovered by Gharib and Roshko [26] and they found the cavity drag in a axisymmetric cavity to be $C_D \sim 0.01$ in shear regime and $C_D \sim 0.3$ in wake regime. They found that there was a threshold level in δ/L where the drag C_D jumped abruptly from the stable area around the shear regime value to a value in the wake regime, thus further strengthening the hypothesis of different types of flow.

To further investigate the flow and acoustic properties of this regime some 2D DNS studies were performed by Larsson [1], Rowley et al [29] and Gloerfelt et al [31]. They all got similar results indicating that the flow was characterized by periodical vortex shedding and in general being much more violent than shear regime flow. Instead of observing the cavity just creating disturbances in the shear layer they found vortices periodically being ejected from the cavity. A dominant frequency was once again found as in shear regime. Rowley et al noted that the frequency of the oscillations does not appear to depend on the Mach number suggesting that the it was the complex motions in the cavity and not a result of a acoustic feedback. Larsson also found that the C_D values were similar to the ones measured by Gharib and Roshko.

In the 2D DNS studies it was suggested that 3D disturbances may have a notable effect on the wake mode. This was investigate by for example Gloerfelt et al [32] and Lawrie [25]. It was found that in 3D DNS studies the flow character of wake regime is suppressed to a state that seems to be more similar to that of shear regime.

4.3 Initial Attempts

When choosing which cavity parameters to use there are some things to consider. There should be good reference data, experimental or DNS. It should be a case that suits the method and it should be feasible to do with the given time and resources. Initially the cavity in Larsson's thesis [1] was chosen. Larsson provides a 2D DS simulation (see section 2.4.1 for a discussion on DS) of a cavity in wake regime and laminar flow. Also Rowley et al does a similar DS runs producing similar results in [29].

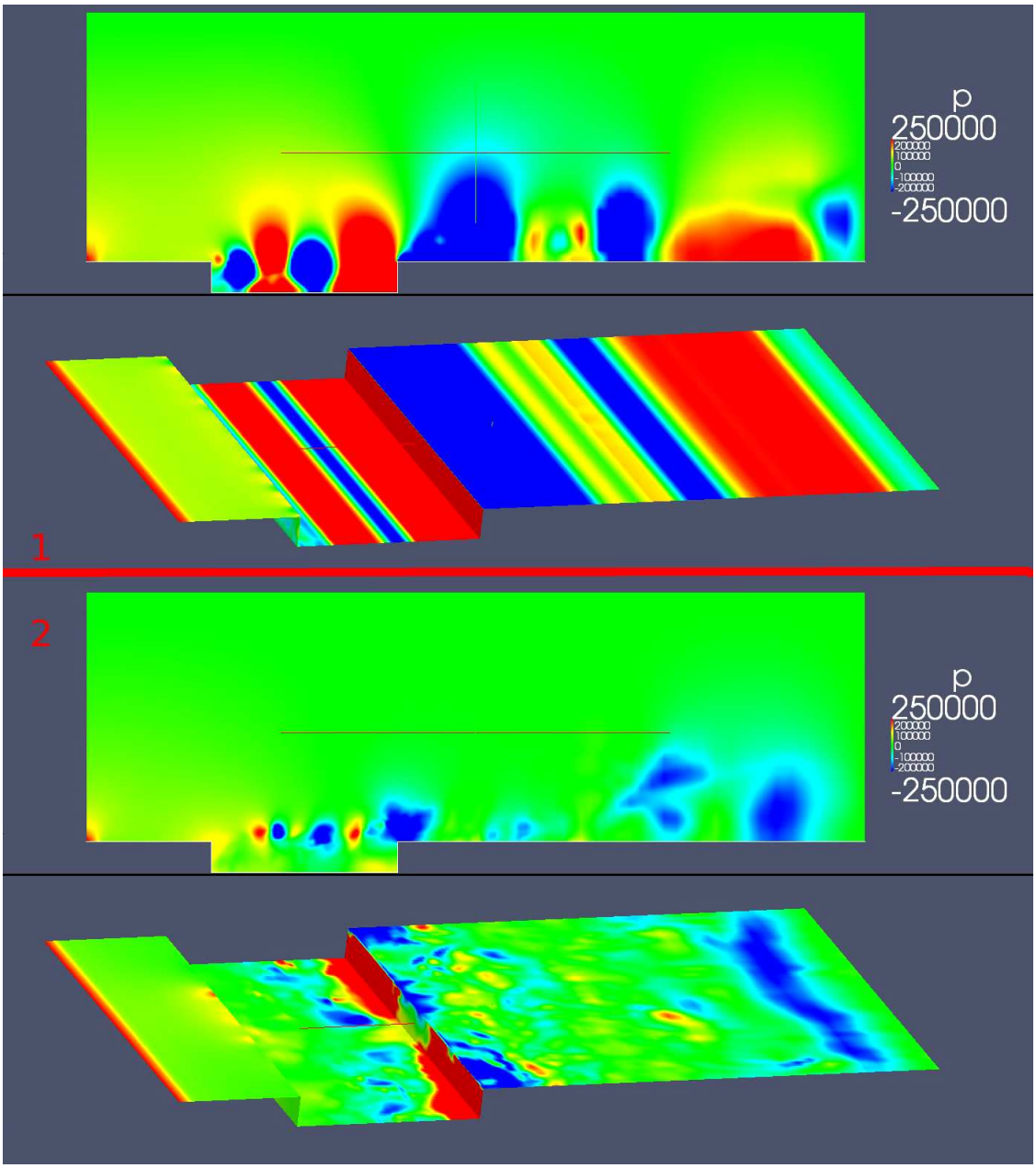

Figure 4.2: Pressure of the wake regime case. The first picture is before the span wise disturbances has broken up the wake regime and the second is after the wake regime has shifted. The pictures are from the same time instants as Figure 4.3.

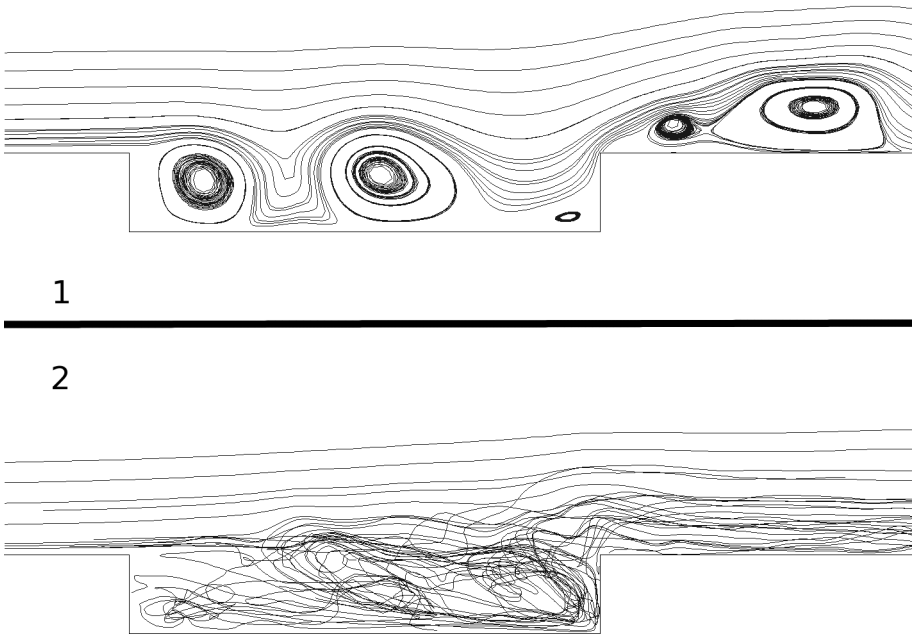

Figure 4.3: Streamlines of the wake regime case. The first picture is before the span wise disturbances has broken up the wake regime and the second is after the wake regime has shifted. The pictures are from the same time instants as Figure 4.2.

It was decided to use a incompressible simulation in 3D. To handle that Larsson's cavity in fact is 2D, at the span wise ends of the domain the boundary conditions were set to be cyclic. The reason for making a 3D simulation was to take into account the 3D nature of the disturbances that occurs. Since the hybrid method does not require that the sound waves to be resolved a much coarser grid can be used, thus making a 3D study feasible. When choosing the initial case it was not known to either author or instructors that a 3D simulation would revert the flow back to a shear regime flow, or at least something similar to shear regime flow. It was only after investigating why the flow behaved so oddly this was discovered.

Figure 4.2 and Figure 4.3 shows the two different characters using pressure and streamlines respectively. In both Figures the half numbered with 1 is from the flow before the span wise disturbances has broken up the quasi-2D flow and the half number 2 is after the quasi-2D flow has been broken up and the vortex shedding has ceased.

It was then decided to change the parameters to a shear regime case. This was done because it turned out to be very hard to find any useful acoustical experimental data for a 3D flow in wake regime with low Mach numbers. In general it became clear that the wake regime was much less understood than it at first appeared to

be. The full method was never run on the case described in this section thus the focus in the remaining thesis will be on the case presented in the next section.

4.4 Test Case

Attempting to use this method on a shear regime case has some implication on the basic assumptions of the method. As described in section 2.2 this assumes that there is no coupling from the acoustics back to the flow. As seen in section 4.2.1 this kind of coupling is believed to cause the entire phenomena of Rossiter modes. Preferably a case which isn't believed to contradict the basic assumptions should be used. Initially this was one of the reasons to use a case in wake regime since it appeared to not be caused by acoustic feedback. However, the problem with wake mode was discovered when there wasn't much time left available to set up a completely new test case, so it was decided to see what results a shear regime case would give.

The specific cavity chosen comes from a NASA study [30]. The study is aimed to give experimental data to validate CAA codes which is exactly what the data will be used as. The cavity parameters are given in table 4.1 with the geometric quantities defined in Figure 4.1. Out the many configurations used in the NASA study this one was chosen because for the following reasons. It was found in the study that since the L/W quota is small, it behaves nearly as a 2D cavity. The Mach number is low enough that a incompressible simulation can be attempted. The acoustic measurements indicate that there is only one frequency that stands out from the background noise and that is the frequency of Rossiter mode $n = 2$. Only one frequency peak makes results easy to compare.

Table 4.1: Parameters of NASA cavity.

L	19.05 mm	L/D	1.5	Re	$1.13 \cdot 10^5$
D	12.70 mm			Ma	0.260
W	101.6 mm	L/W	0.1875	U	89.0 m/s
δ	2.309 mm	δ/L	0.121		

4.5 CFD Model

For the CFD simulation the software OpenFOAM was used (see section 3.2). The incompressible solver pisoFoam was used with the additional code for the source term described in section 3.4. Since the flow is turbulent, a turbulence model was needed. To make sure that as much of the vortices as possible are resolved LES was

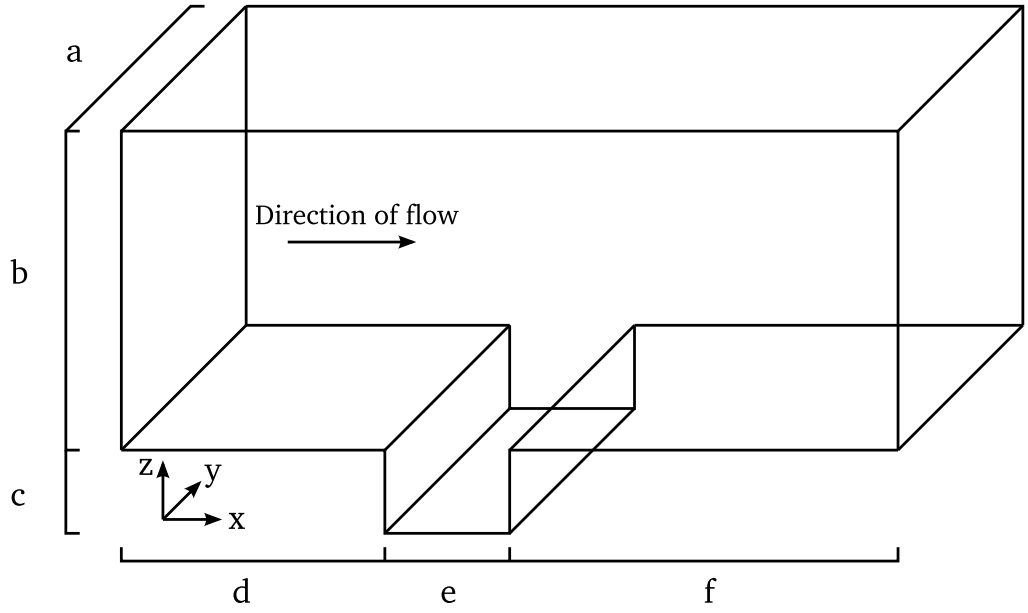

Figure 4.4: Mesh geometry.

chosen. The LES model chosen was Smagorinsky and the reason for this was mainly simplicity. The Smagorinsky coefficient C_k was kept at its default value $C_k = 0.094$.

The inlet boundary condition was a straight velocity profile. In other words the same fluid velocity was given over the entire inlet and the only non zero component was in the x-direction. Such a flat velocity profile does not contain any turbulence by itself. The turbulence is instead triggered as the boundary shear layer near the wall begins to grow. By adjusting the distance from the inlet to the leading edge of the cavity the boundary layer thickness was matched to the one in the NASA experiment. The outlet boundary condition for the velocity was zero gradient and on the walls the no slip boundary condition was used. The pressure was set to zero at the inlet and zero gradient at the outlet and walls. At the sides of the domain (the extremes in the y-direction) the boundary condition was set to cyclic. Since the NASA study has found that for these geometrical parameters the cavity behaved roughly two dimensional and by doing it this way the whole cavity did not have to be resolved.

The mesh was generated using the built in tool `blockMesh`, which is as the name implies a block mesher. The mesh geometry is shown in Figure 4.4 with the parameters given in table 4.2. The mesh was stretched so that there are many cells for the shear layer and in the cavity. The shear layer has about 15 cells in the z-direction near the upstream edge of the cavity and the cavity itself contains 180'000 cells. About 1.1 million hexahedra cells were used for the whole mesh.

The time discretization scheme used for the time derivative was a second order implicit scheme, known in OpenFOAM as `backward`. The discretization in space

Table 4.2: Parameters of the CFD mesh.

Expressed in units of $D = 12.7$ mm		
$a = 4\ D = W$	$b = 6\ D$	$c = 1\ D = D$
$d = 7\ D$	$e = 1.5\ D = L$	$f = 13.5\ D$

used those called `Gauss linear` in OpenFOAM. This means Gaussian integration using linear interpolation giving second order schemes for the gradient, laplacian, divergence and convection terms. For the laplacian discretization the `corrected` scheme, which is a conservative scheme, was used. For more information about the discretization schemes see the OpenFOAM documentation at [18]

4.6 FEM Model

The acoustic FEM solver was a extended and modified version of CALFEM (see section 3.3). The mesh was generated using OpenFOAM's tool blockMesh and then converted using the purpose written converter described in section 3.5. The mesh consisted of 80000 hexahedral cells and covered a smaller domain than the CFD model. The geometry is the same as in the CFD model (see Figure 4.4) but with the geometrical parameters given in table 4.3. The walls were modeled as perfectly reflecting hard surfaces while the other boundaries used the absorbing boundary condition described in section 2.3. The sides of the cavity that was given a cyclic boundary condition in the CFD simulation was also given the absorbing boundary condition. This was done to save time and it is not expected to affect the result much if one looks near the middle of the domain in the y-direction. It should be possible to set the boundary condition to cyclic in CALFEM and doing so should improve the results.

Table 4.3: Parameters of the FEM mesh.

Expressed in units of $D = 12.7$ mm		
$a = 4\ D = W$	$b = 6\ D$	$c = 1\ D = D$
$d = 4\ D$	$e = 1.5\ D = L$	$f = 4\ D$

The acoustic domain does not really extend to the far field. In fact the acoustic domain is smaller than the fluid domain, which probably would not be the case in a real world application. This was not considered to affect the tested methodology much and it had the benefit of allowing the FEM computation to run in just a few hours on a single desktop computer.

Chapter 5

Results

5.1 Mean Flow Fields

In general the flow can be described as a flat plate boundary layer flow which is not affected much by the cavity it passes over. Figure 5.1 shows the x-component (stream wise) of the mean velocity field. There it can be seen how the boundary layer develop from the flat velocity profile supplied to the inlet. The cavity does not affect the velocity profile much. This can also be seen in Figure 5.2 where the mean streamlines are shown. There is one large vortex filling nearly the whole cavity. There is also a hint of a small secondary vortex at the bottom-upstream corner of the cavity.

The mean pressure field in Figure 5.3 shows the expected area of increased pressure near the inlet as a result of the flat inlet profile being slowed near the wall when forming the boundary layer. It also shows an area of higher pressure near the downstream edge of the cavity which is also expected. The scale of Figure 5.3 is however set to highlight both of the mentioned areas. The higher pressure at the inlet is at its highest value actually one order of magnitude larger than the one near the downstream edge of the cavity. If the scale is modified as in Figure 5.4 a concerning feature emerges. Above the leading edge a pillar like feature exists that really shouldn't be there. The cause of this is not known. The best guess is that there is some kind of problem in OpenFOAM. When creating the mesh with `blockMesh` the domain was divided into four different regions. The pillar exists on the border between two of these regions. For some reason it is suspected that there has been some problem at the border between the two regions in OpenFOAM.

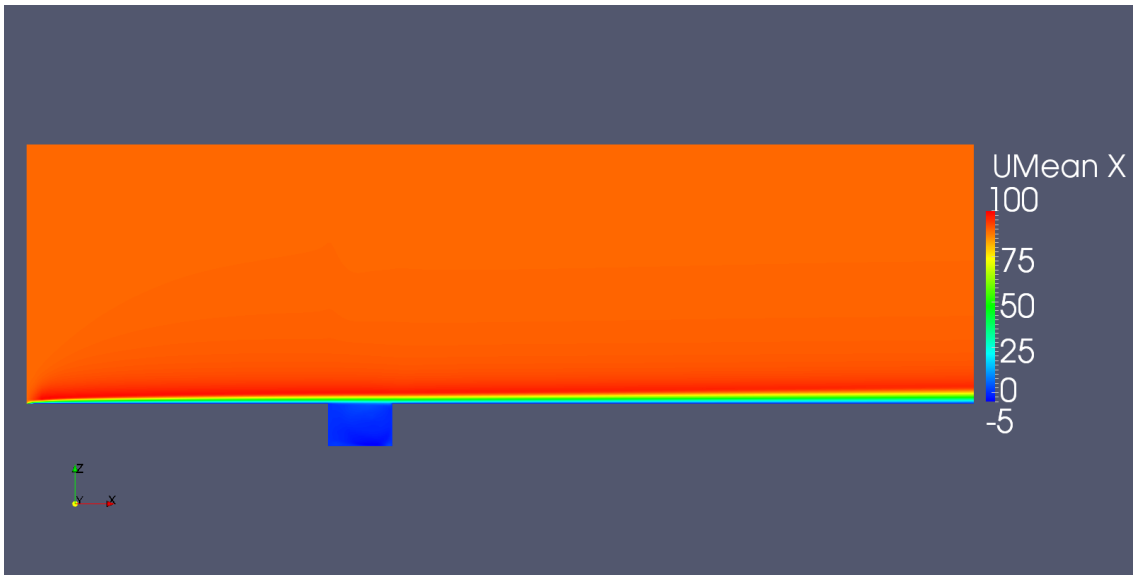

Figure 5.1: Mean x-component of the velocity in m/s.

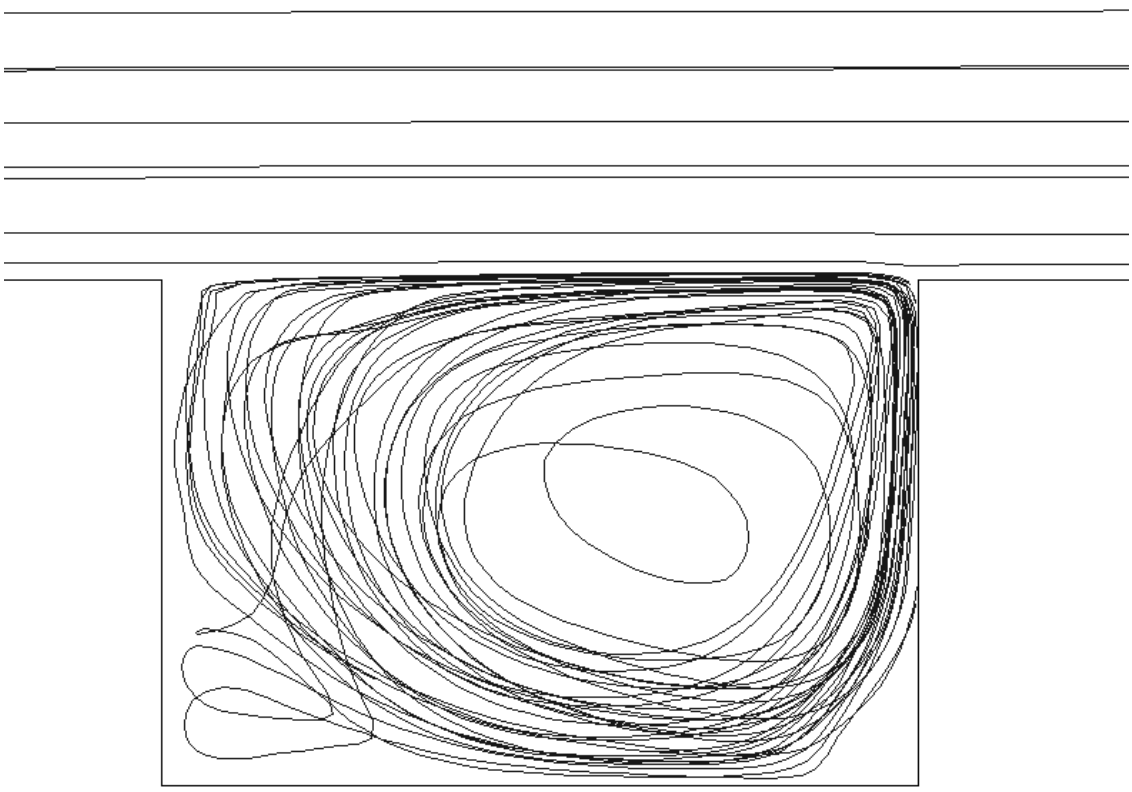

Figure 5.2: Mean streamlines.

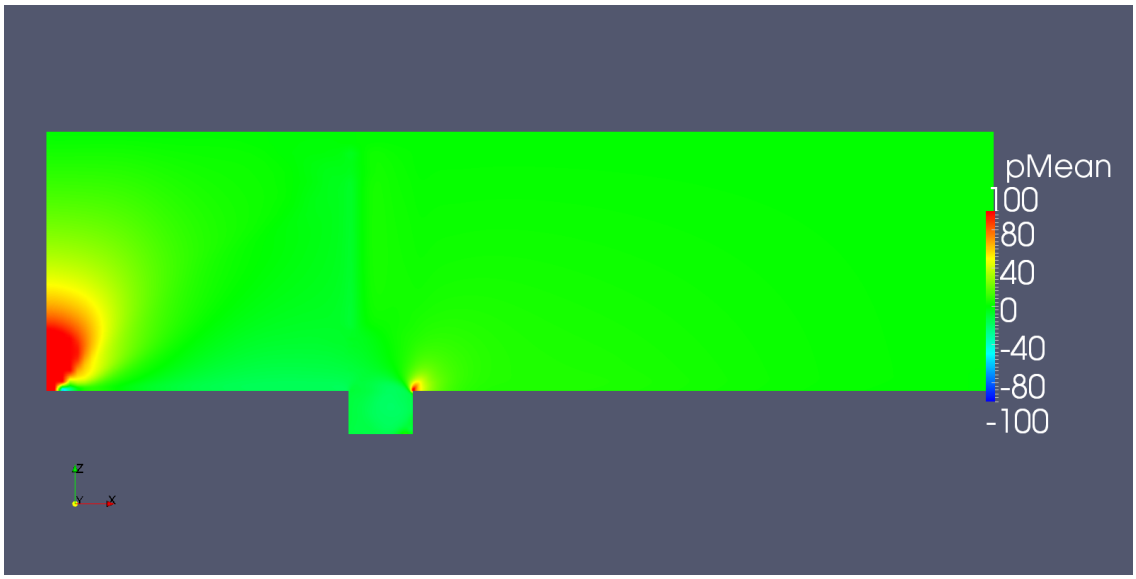

Figure 5.3: Mean pressure in Pa. Note that the scale saturated to reveal more structures. In the high pressure zone near the inlet the pressure reaches just above 1500 Pa.

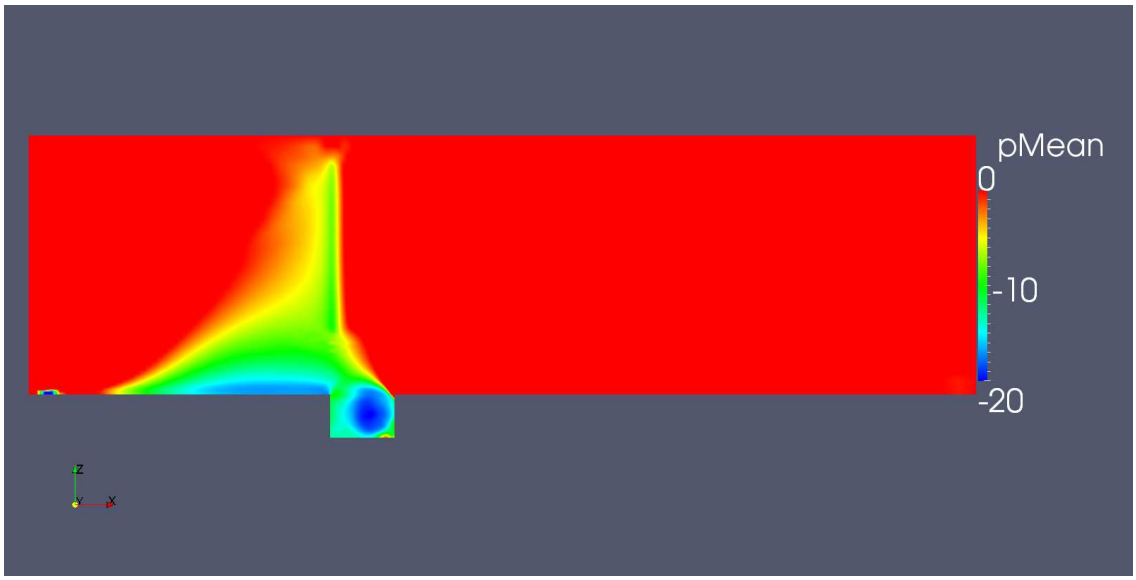

Figure 5.4: Mean pressure in Pa with the scale skewed in order to reveal the pillar like structure above the upstream cavity edge.

5.2 Cavity Drag

The drag coefficient C_D is defined as

$$C_D = \frac{F}{\frac{1}{2}\rho U_\infty^2 A} \tag{5.1}$$

where F is the force in the x-direction inside the cavity, U_∞ is the free stream velocity and A is the area of one of the vertical walls inside the cavity ($A = D \cdot W$). Figure 5.5 shows the cavity drag after the simulation has entered steady state. First note the scale of the drag. It oscillates slightly around $C_D \approx 1.5 \cdot 10^{-5}$. For non-oscillating flows Gharib and Roshko [26] found experimentally $C_D \approx 1 \cdot 10^{-4}$. They did however use an axisymmetric cavity with water at low velocities.

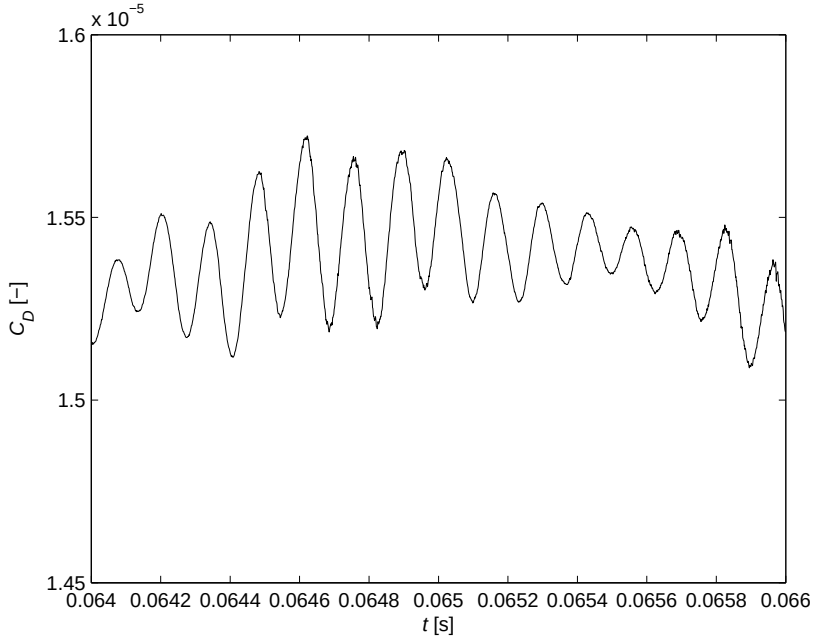

Figure 5.5: Cavity drag in time domain.

Figure 5.6 shows the frequency spectra of C_D. On the horizontal axis is the Strouhal number as defined in (4.2). Before calculating this spectra the much dominant dc offset was removed so that the other frequencies can easier be observed. As Figure 5.5 hinted with one frequency being clearly dominant, there is only one peak and some low frequency noise. The low frequency noise may come from transients that has yet to die out. If the frequency of the third Rossiter mode is calculated by using (4.1) with $Ma = 0$ for incompressible simulation, this gives the value $St_L = 1.57$ which is a good match to the frequency obtained from Figure 5.6. Despite this it is not believed that the coupling phenomena that is associated with the shear regime is responsible. One argument, the actual level of cavity drag indicates no oscillations, has already been mentioned. More arguments will follow below.

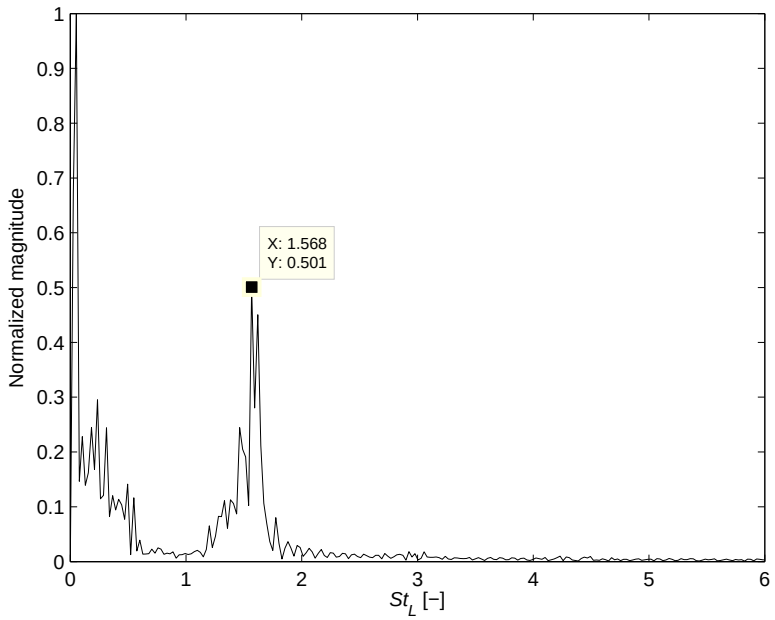

Figure 5.6: Cavity drag in frequency domain with the dc offset removed, St_L is the non-dimensionalized frequency.

5.3 Acoustical Sources

Figure 5.7 shows the acoustical source terms computed according to (2.7) at two different times and the difference between the two different times. The scale in Figure 5.7 is saturated in several areas in the two upper pictures, for example the area near the inlet and the area at the downstream upper corner of the cavity. In fact, the amplitude of the acoustical sources near the downstream upper cavity corner is two orders of a magnitude larger than at the scale permits. The scale is set this way so that the moving structures can be seen. The bottom picture in Figure 5.7 removes everything that is stationary and reveals that the wave like pattern above the cavity is indeed moving. It is moving to the right with the flow. These waves are the part that will make a difference to the acoustical calculations. All stronger areas of sources does not move or oscillate in any way. This give them a frequency content consisting almost exclusively of the frequency zero. Since pressure fluctuations of the frequency zero doesn't cause any sound the scale in Figure 5.7 has been set to highlight the moving waves which do cause sound.

The pillar structure above the upstream cavity wall that turned up in the pressure field (see Figure 5.4) is once again visible. It is however stationary and does not really contribute to the sound since the frequency is zero as motivated above.

Unfortunately the wave pattern is not believed to be caused by the physical reason of the cavity oscillation. The wave pattern does not seem to originate from the

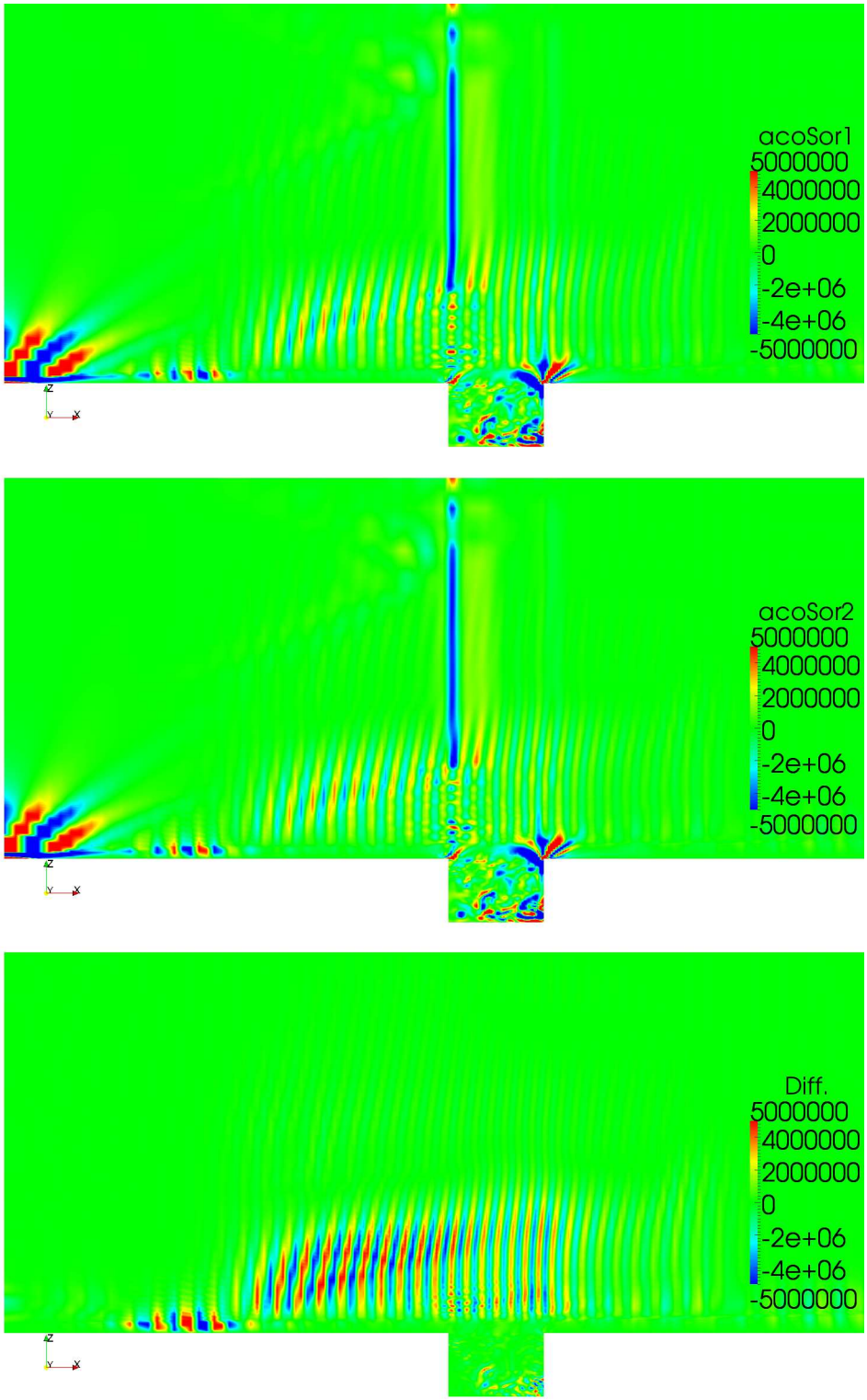

Figure 5.7: The upper two pictures are the acoustical source terms computed according to (2.7) in $\mathrm{kg\,m^{-3}\,s^{-2}}$ for two times separated by $\Delta t = 7 \cdot 10^{-5}$ s. The bottom picture is the first picture substracted from the second picture.

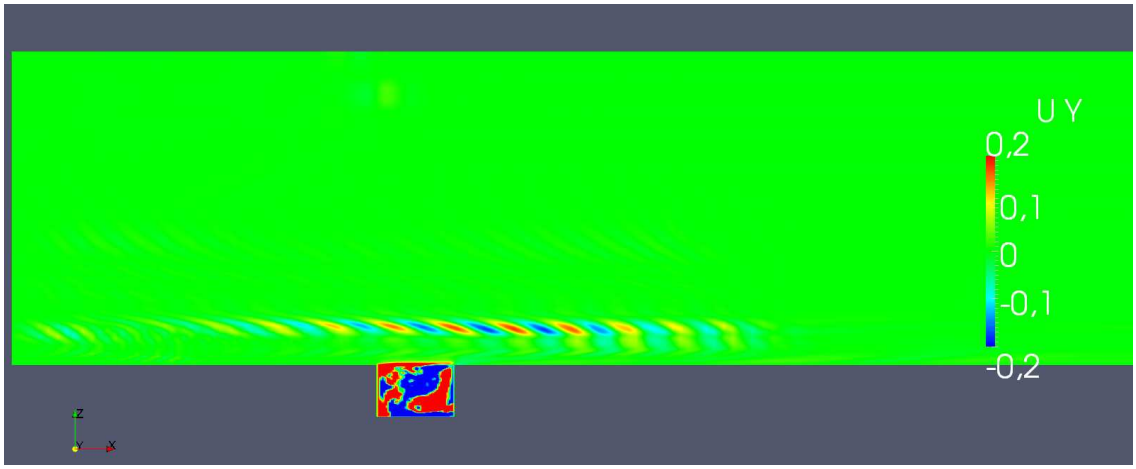

Figure 5.8: The y-component of the velocity field for one time instant in m/s.

cavity, but rather from the inlet. Figure 5.8 shows the y-component of the velocity field for one time instant. Once again the scale is set to reveal the structures above the cavity, thus saturating the patterns inside the cavity. The vortices above the cavity travel with the flow in the same way that the acoustical sources do in Figure 5.7 and is believed to be the cause for the wave pattern in the sources. This periodic vortex structure seems to be caused by the boundary conditions together with the nature of the incompressible solver forcing the frequency on top of the shear layer. They do not seem to originate from the cavity but rather from the inlet. They also travel above the shear layer while the intended physical phenomena is suppose to originate from the shear layer. Even though it seems that the acoustical source terms appears to be generated in an unphysical way they will be used in the further investigation of the results.

The effect of interpolation can be seen in Figure 5.9. A lot of detail in the cavity has been filtered out by the interpolation. These sources in the cavity were mostly dominated by the low frequencies. The filtering that removed much of them is only expected to have minor effect on the lower frequencies. The wave pattern is fairly well resolved. It does appear to have lost some strength. Since the shape of the pattern is correct it should give the same acoustical patterns but maybe reduce the sound amplitude due to the strength difference.

Figure 5.10 shows the magnitude of the acoustical sources in the frequency domain for $St_L = 1.46$, transformed according to section 3.7 (after interpolation). They cover approximately the area covered by the wave pattern in Figure 5.7. Figures 5.12 and 5.13 show the frequency spectra for observers A and B defined in Figure 5.11. Note the different scales in Figures 5.12 and 5.13. Observer A, located in the wave pattern above the cavity, has a peak near the same frequency as the peak in the cavity drag spectra. This suggests that it is the same phenomena causing both peaks. Observer B located near the downstream edge of the cavity shows a massive dominance of the zero frequency and not much else.

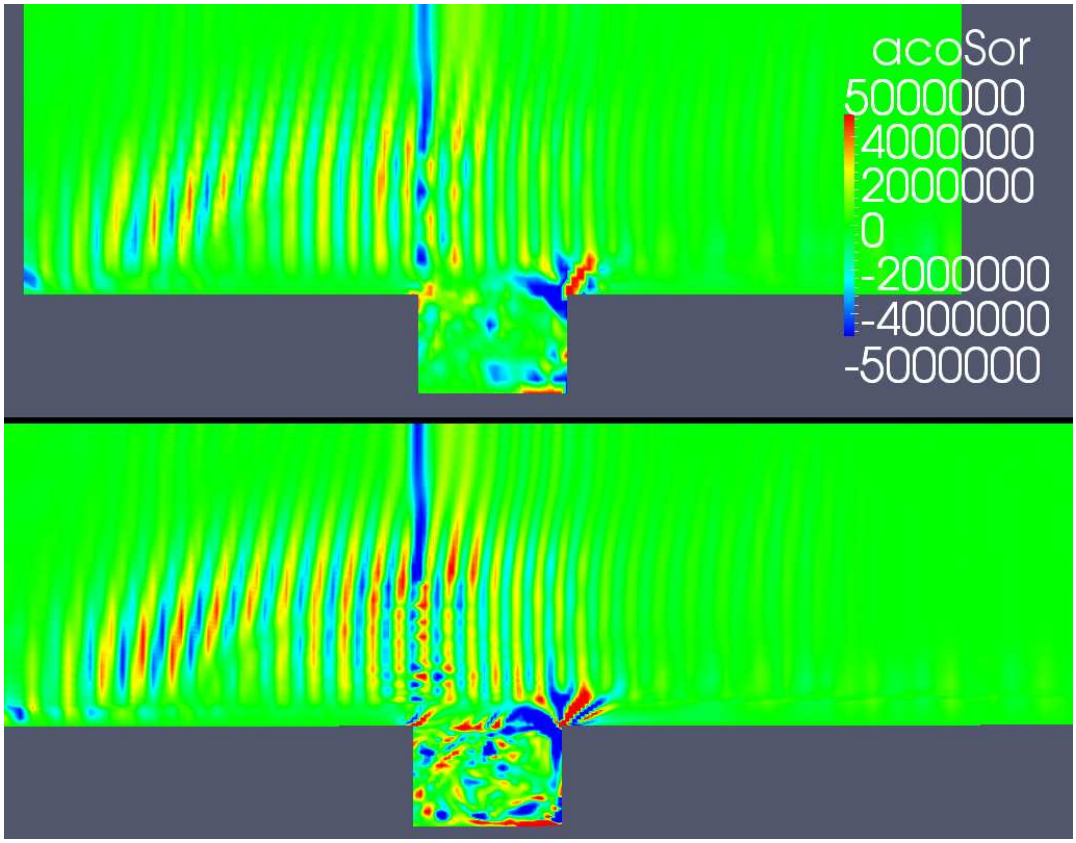

Figure 5.9: Comparison between the acoustical source before and after the interpolation. The interpolated data is on the top. The acoustical sources are in $\mathrm{kg\,m^{-3}\,s^{-2}}$.

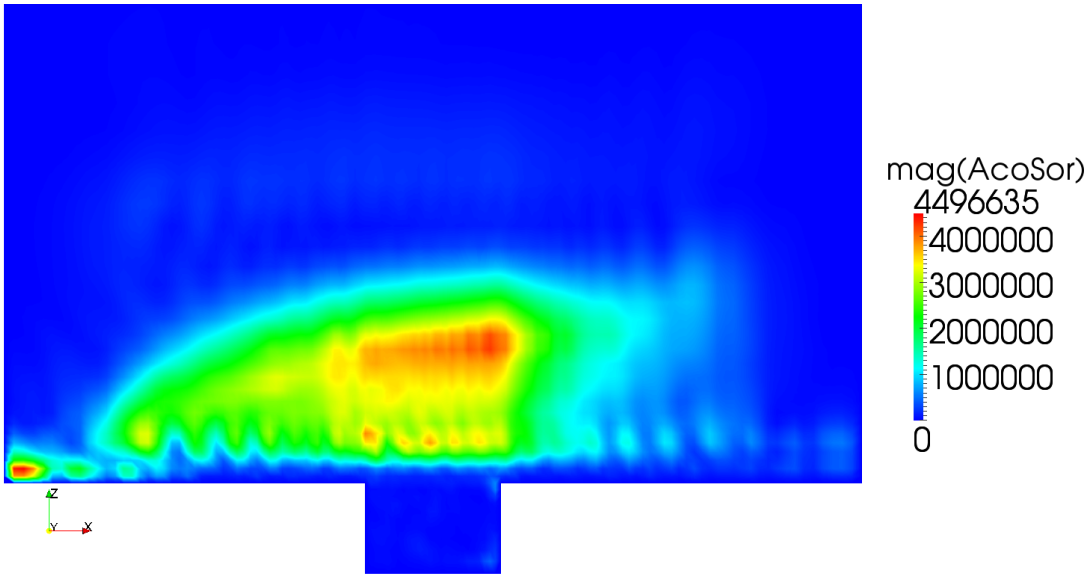

Figure 5.10: The magnitude of the acoustical sources transformed to frequency domain for the non-dimensinalized frequency $St_L = 1.46$ in $\mathrm{kg\,m^{-3}\,s^{-2}}$.

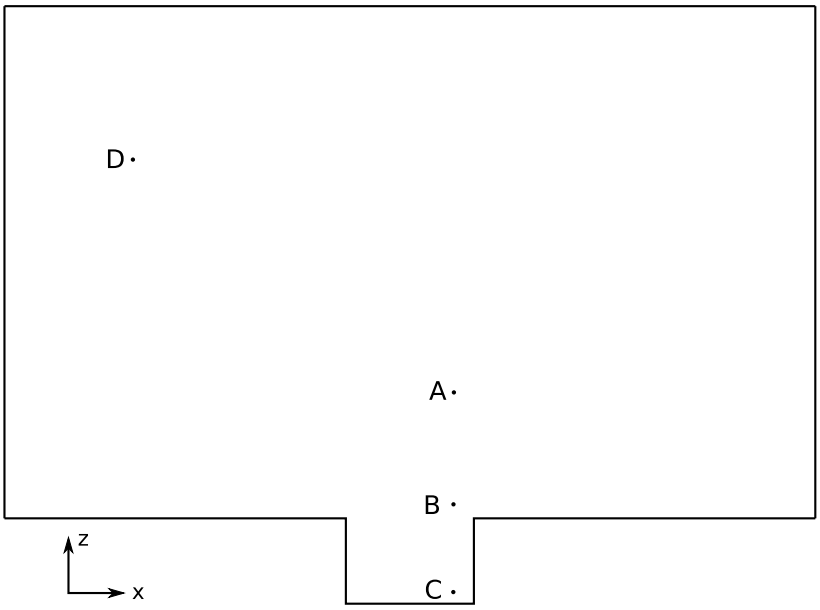

Figure 5.11: Four observer points defined in the acoustical domain. All observers are located in the middle of the domain in the y-direction. The Figure is to scale.

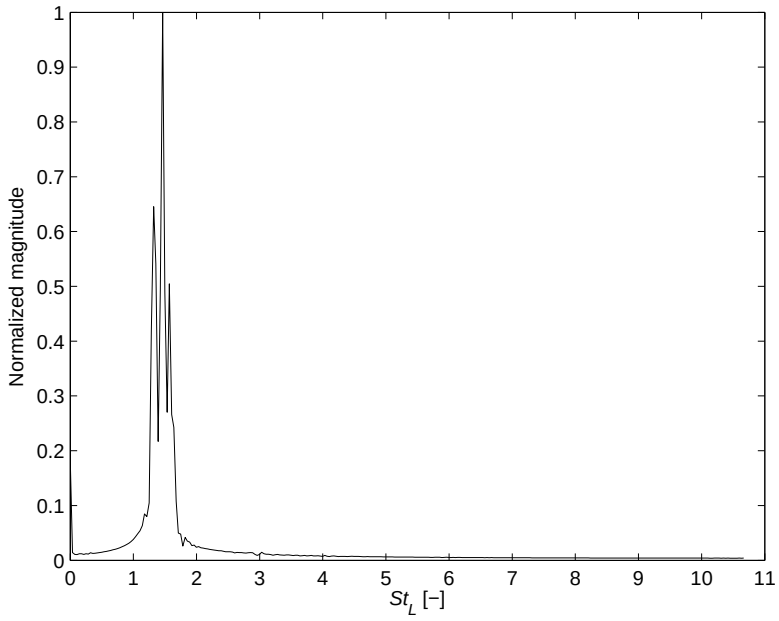

Figure 5.12: Spectra of the acoustical source term for observer A.

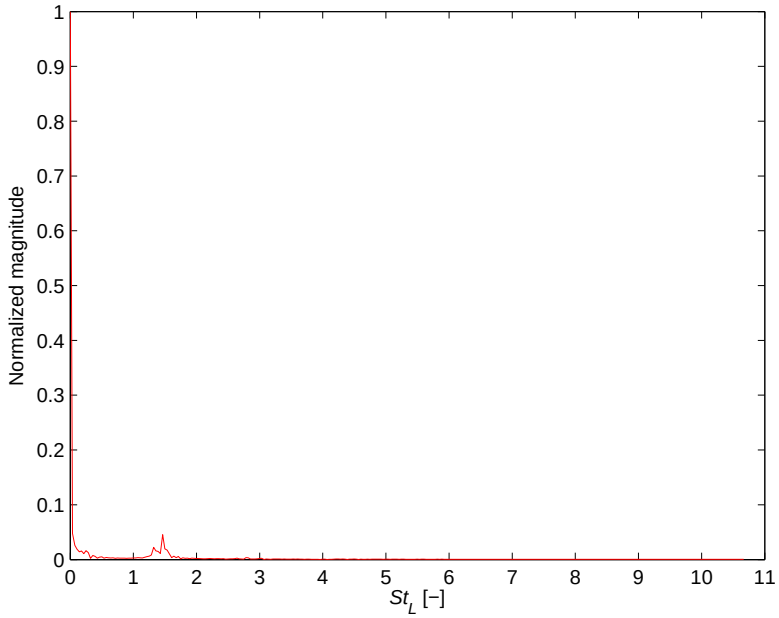

Figure 5.13: Spectra of the acoustical source term for observer B.

5.4 Acoustical Results

Figure 5.14 shows the sound pressure level for $St_L = 1.46$, at the same frequency as in Figure 5.10. The sound levels in the middle slice of the domain in the xz-plane ar given in Figure 5.14. This slice is the most representative one since the boundaries on the sides are set to absorbing boundary condition rather than the physically more correct cyclic boundary condition. Figure 5.15 shows the sound pressure level in the yz-plane. The sound level drops off a bit at the sides indicating that the absorbing boundary condition is working like intended. Figure 5.16 gives the same thing as Figure 5.14, but with the amplitude of the pressure fluctuations in linear scale for easier comparison to 5.10. The acoustic solver appears to be working properly. The walls seems to give reflection and the other boundaries seems to absorb everything. It is also important to remember that the phase of the of the sources in each node is also taken into account by acoustical solver when comparing the Figure 5.10 and 5.16. Two nearby sources with opposite phase can cancel each other out for large portions of the domain.

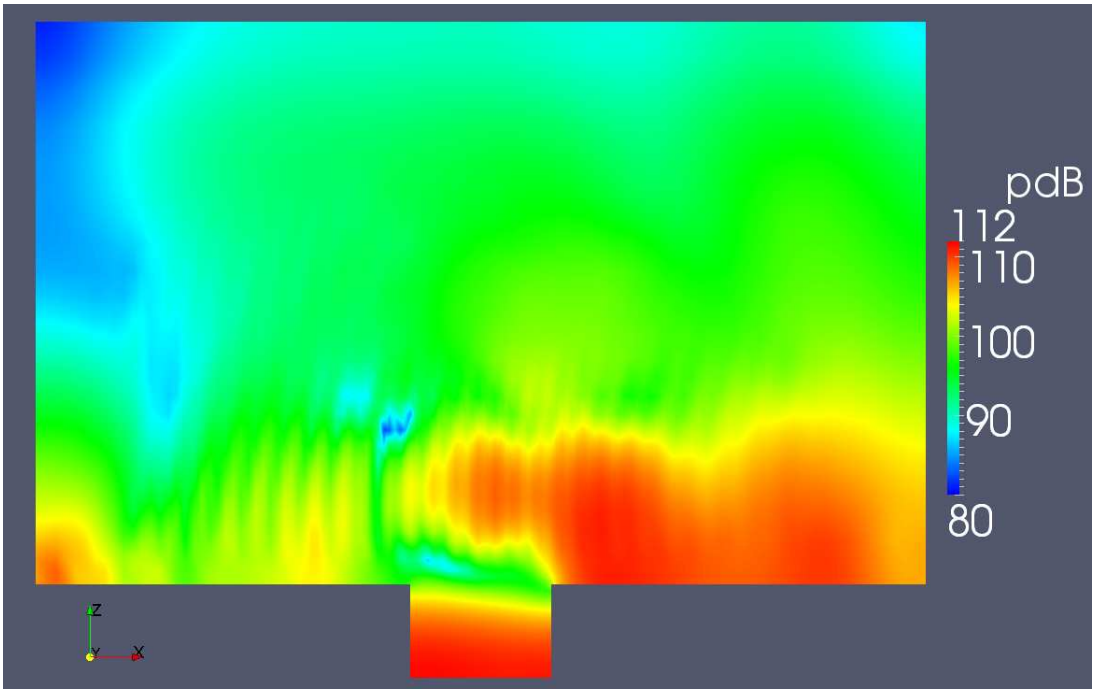

Figure 5.14: Sound pressure levels in dB (ref 20 μPa) for the frequency $St_L = 1.46$.

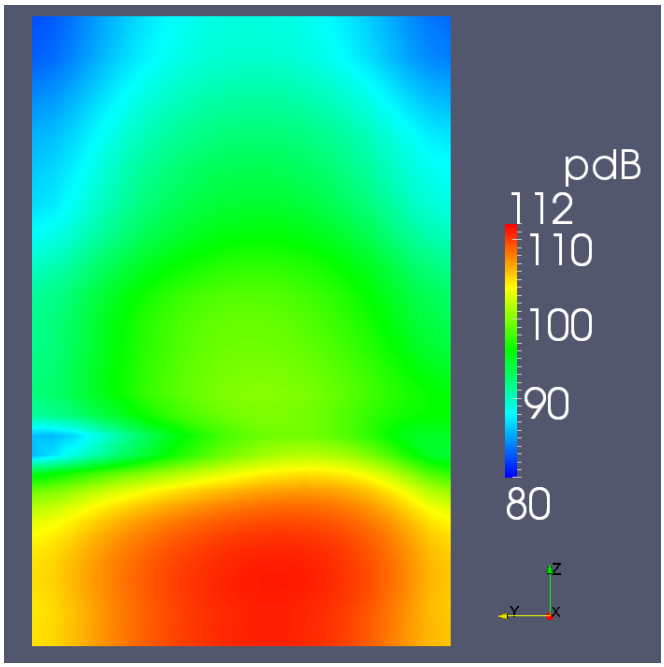

Figure 5.15: Sound pressure levels in dB (ref 20 μPa) in the yz-plane, 0.5 D downstream of the cavity for the frequency $St_L = 1.46$.

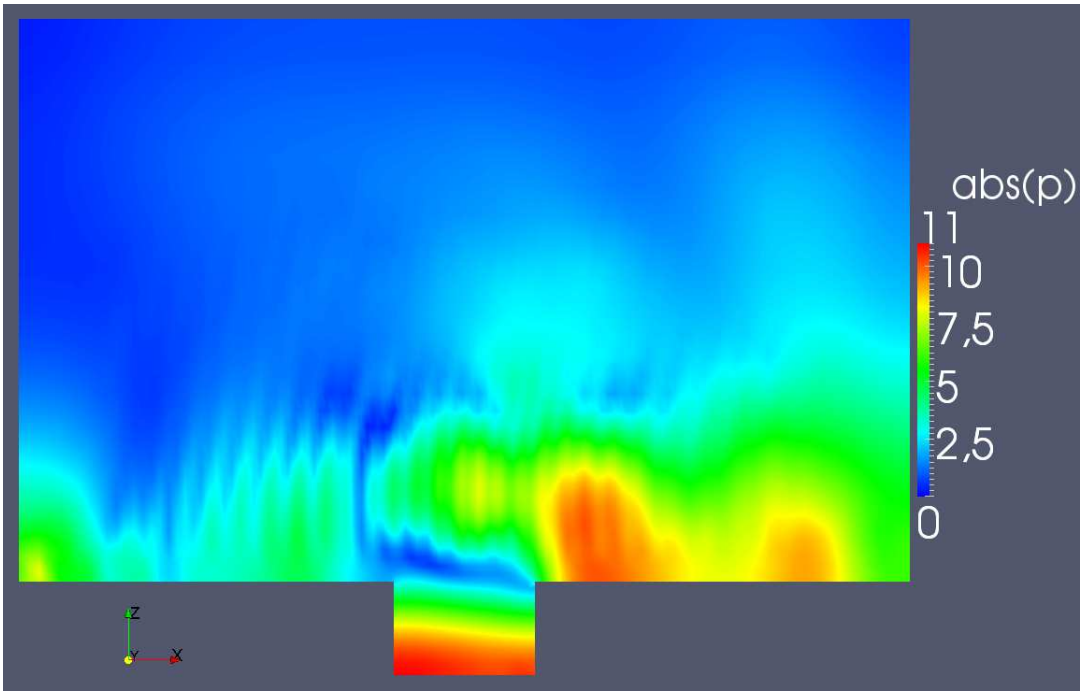

Figure 5.16: Magnitude of pressure fluctuations in Pa for the frequency $St_L = 1.46$.

The data that the acoustic solver gets to work with is most likely unphysical, but with the data given it seems to work as intended. Figures 5.17 to 5.20 show the frequency spectra of acoustic pressure at the observers A-D as defined in Figure 5.11. Once again there is a peak similar to the one for the cavity drag in Figure 5.6.

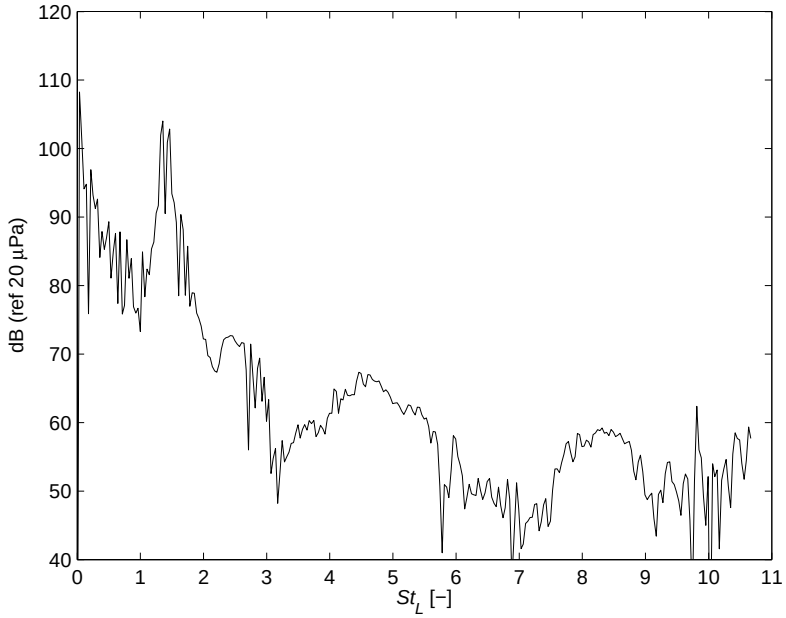

Figure 5.17: Spectra of the sound pressure level for observer A.

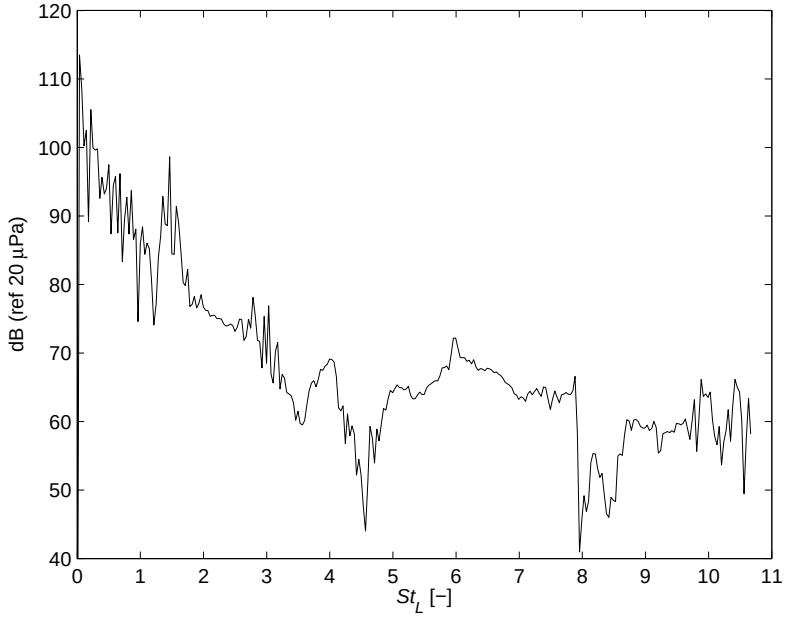

Figure 5.18: Spectra of the sound pressure level for observer B.

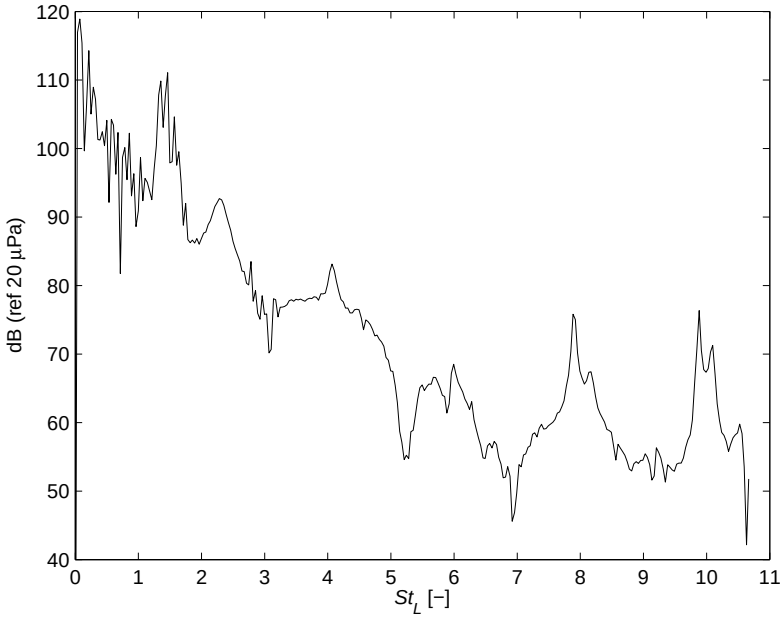

Figure 5.19: Spectra of the sound pressure level for observer C.

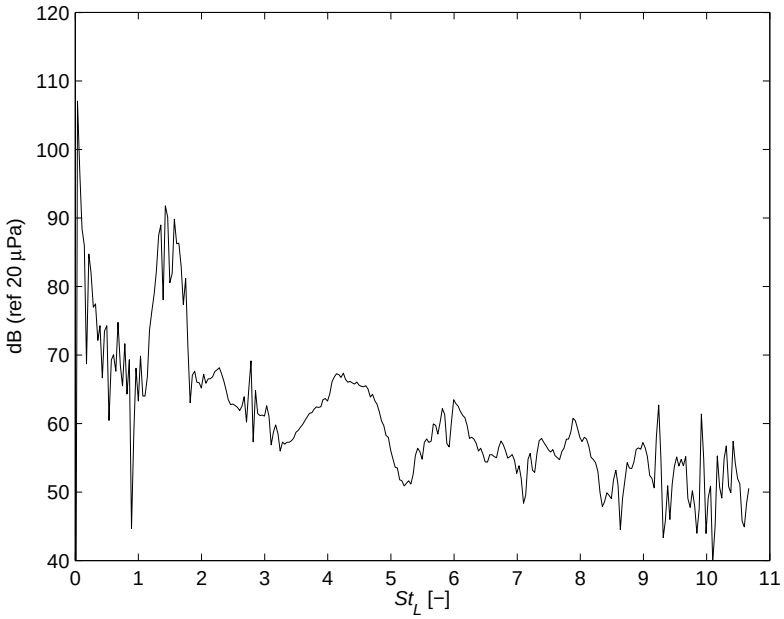

Figure 5.20: Spectra of the sound pressure level for observer D.

Chapter 6

Conclusions and Future Work

Three objectives were set up for this thesis. The first objective, to see how and if a hybrid CAA method can be used with CALFEM has been well covered, mostly in the theory chapter. The method of using Lighthill's acoustical source term with a FE formulation does not appear to be commonly used but some validation can be found in the literature, for example in [2, 33]. With the suitable method found and confirmed to be working by other studies this objective is considered to be accomplished.

The proposed method has been implemented and the whole computational process has been performed. This means that the second objective has also been met. The implementation is spread out in several small programs. While this gives flexibility the user must know details in the process, like which order the programs should be run and in some cases which files must be adjusted or copied for the process to work properly. The extent to which the process has been generalized and the fault that tolerance has been implemented varies. One can view the implementation as a proof of concept rather than a completed software package for a OpenFOAM and CALFEM interaction for hybrid CAA method.

The third and final objective was to setup a case to test and validate the implemented method. While a case was indeed setup and tested the choice of test case unfortunately turned out be a bad one. The method can in no way be considered to be validated in this thesis. The problem lies in the chosen CFD model and the hybrid method simply isn't suited for this problem. Since the result is that the method fails, these limitations in the method can be confirmed.

Even though the test case gave results that are believed to be unphysical the individual steps of the implementation appears to work as intended. Further testing is required before this can be confirmed however.

The most obvious next step is to take the implemented method and test it on a different and more suitable case so that it can be validated and satisfy the third

objective of the thesis. If more time would have been available for the thesis this would have been done.

The code that implements the method could be more generalized and polished. For example the mesh converter could be written to handle all types of elements that are supported by both OpenFOAM and CALFEM. More steps can be automated. It should be possible to add the relevant parts of the CALFEM code base to OpenFOAM. CALFEM has as mentioned already been ported to Python. Including the CALFEM code in OpenFOAM would make it possible (or at least much easier) to run the whole simulation in one single run and removes the requirement to use Matlab. It also opens the possibility to attempt to couple the acoustics with the CFD simulation.

Bibliography

[1] J. Larsson, *Computational Aero Acoustics for Vehicle Applications*, PhD Thesis, Department of Thermo and Fluid Dynamics, Chalmers University of Technology, (2002).

[2] M. Escobar, *Finite Element Simulation of Flow-Induced Noise using Lighthill's Acoustic Analogy*, PhD Thesis, Der Technischen Fakultät der Universität Erlangen-Nürnberg, (2007).

[3] M. J. Lighthill, *On Sound Generated Aerodynamically. I. General Theory*, Proceedings of the Royal Society London, 211 (1952), 564-587.

[4] J. E. Ffowcs-Williams, D. L. Hawkings, *Sound Generation by Turbulence and Surfaces in Arbitrary Motion*, Philosophical Transactions of the Royal Society of London (1969), 321-342.

[5] A. Oberai, F. Roknaldin, T. Hughes, *Computational procedures for determining structural-acoustic response due to hydrodynamic sources*, Comp. Methods Appl. Mech. Engineering 190 (2000), 345-361

[6] S. Caro, R. Sandboge, J. Iyer, Y. Nishid, *Presentation of a CAA Formulation Based on Lighthill's Analogy for Fan Noise*, Fan Noise, (2007)

[7] D. G. Crighton, *Aeronautical Acoustics: Mathematics Applied to a Major Industrial Problem*, ICIAM '87: proceedings of the First International Conference on Industrial and Applied Mathematics, Paris (1987)

[8] A. Hirschberg, S.W. Rienstra, *An introduction to aeroacoustics*, Dept. of App. Physics and Dept. of Mathematics and Comp. Science, Eindhoven University of Technology, (2004)

[9] S. Slimon, M. Soteriou, D. Davis, *Development of Computational Aeroacoustics Equations for Subsonic Flows Using a Mach Number Expansion Approach*, Journal of Computational Physics 159 (2000), 377-406

[10] N. Ottosen, H. Petersson, *Introduction to the Finite Element Method*, Prentice Hall, New York, (1992).

[11] P-A. Wernberg, *Structure-Acoustic Analysis; Methods, Implementations and Applications*, PhD thesis, Division of Structural Mechanics, Lund University (2006)

[12] S. Pope, *Turbulent Flows*, Cambridge University Press, Cambridge, (2009)

[13] S. Caro, P. Ploumhans, X. Gallez, *Implementation of Lighthill's Acoustic Analogy in a Finite/Infinite Elements Framework*, Proceedings of 10th AIAA/CEAS Aeroacoustics Conference 2004, Manchester, UK, (2004)

[14] C. Bailly, D. Juvé, *Numerical Solution of Acoustic Propagation Problems Using Linearized Euler Equations*, AIAA Journal 38 (2000) no. 1

[15] C. Bogey, C. Bailly, D. Juvé, *Computation of Flow Noise Using Source Terms in Linearized Eulers Equations*, AIAA Journal 40 (2002), no. 2

[16] R. Ewert, W. Schröder, *Acoustic perturbation equations based on ow decomposition via source ltering*, Journal of Computational Physics 188 (2003), 365-398

[17] J. H. Seo, Y. J. Moon, *Linearized perturbed compressible equations for low Mach number aeroacoustics*, Journal of Computational Physics 218 (2006), no. 2, 702-719

[18] *OpenFOAM Webpage*, `http://www.openfoam.com`, retrieved 2010-12-07, se ev. Lorentzons rapport, referens nr65.

[19] B. Smith, *A Quick Guide to GPLv3*, `http://www.gnu.org/licenses/quick-guide-gplv3.html`, Free Software Foundation, Inc, retrieved 2010-12-07.

[20] P-E. Austrell, O. Dahlblom, J. Lindemann, A. Olsson, K-G. Olsson, K. Persson, H. Petersson, M. Ristinmaa, G. Sandberg, P-A. Wernberg, *CALFEM - A Finite Element Toolbox*, KFS i Lund AB, Lund, (2004)

[21] *CALFEM*, `http://sourceforge.net/projects/calfem/`, retrieved 2010-12-07.

[22] A. Ottosson, *Implementaion of CALFEM for Python*, MSc. Thesis, Div. of Structural Mechanics, LTH, Lund University, (2010)

[23] *FFTW Webpage*, `http://www.fftw.org/`, retrieved 2010-12-07

[24] C. Moler, S. Eddins, *Faster Finite Fourier Transforms, MATLAB 6 incorporates FFTW*, Mathworks newsletter, `http://www.mathworks.com/company/newsletters/news_notes/clevescorner/winter01_cleve.html`, retrieved 2010-12-07

[25] D. Lawrie, *Investigation of cavity flows at low and high Reynolds numbers using computational fluid dynamics*, PhD Thesis, University of Glasgow (2004)

[26] M. Gharib, A. Roshko, *The effect of flow oscillations on cavity drag*, Journal of Fluid Mechanics, 177 (1987). 501-530

[27] J. E. Rossiter, *Wind tunnel experiments on the flow over rectangular cavities at subsonic and transonic speeds*, Technical report 3438, Aeronautical Research Council Reports and Memoranda (1964)

[28] G. A. Brès, *Numerical Simulations of Three-Dimensional Instabilities in Cavity Flows*, PhD Thesis, California Institute of Technology Pasadena, California (2007)

[29] C. W. Rowley, T. Colonius, A. J. Basu, *On self-sustained oscillations in two-dimensional compressible flow over rectangular cavities*, Journal of Fluid Mechanics 455 (2002), 315-346

[30] K. K. Ahuja, J. Mendoza, *Effects of cavity dimesnions, boundary layer, and temperature on cavity noise with emphasis on benchmark data to validate coumptational aeroacoustic codes*, NASA, CR-4653 (1995)

[31] X. Gloerfelt, C. Bailly, D. Juvé, *Direct computation of the noise radiated by a subsonic cavity ow and application of integral methods*, Journal of Sound and Vibration, 266 (2003) 119-146

[32] X. Gloerfelt, C. Bogey, C. Bailly, D. Juvé, *Aerodynamic noise induced by laminar and turbulent boundary layers over rectangular cavities*, American Institue of Aeronautics and Astronautics, 2002-2476 (2002)

[33] R. Sandboge, S. Caro, P. Ploumhans, R. Ambs, B. Schillemeit, K. B. Washburn, F. Shakib, *Validation of a CAA formulation based on Lighthills Analogy using AcuSolve and Actran/LA on an Idealized Automotive HVAC Blower and on an axial fan*, American Institue of Aeronautics and Astronautics, 2002-2692 (2006)